Correlated Noise Effects in Spacecraft Telemetry Arraying

by

Pravin Anand Vazirani

Submitted to the Department of Electrical Engineering and Computer Science
in partial fulfillment of the requirements for the degree of

Master of Science in Electrical Engineering and Computer Science

at the

MASSACHUSETTS INSTITUTE OF TECHNOLOGY

May 1995

Author .....
Department of Electrical Engineering and Computer Science
May 18, 1995

Certified by .....
Robert Gallager
Professor
Thesis Supervisor

Certified by .....
Biren Shah
Company Supervisor
Thesis Supervisor

Accepted by .....
Frederic R. Morgenthaler
Chairman, Departmental Committee on Graduate Students

Correlated Noise Effects in Spacecraft Telemetry Arraying

by

Pravin Anand Vazirani

Submitted to the Department of Electrical Engineering and Computer Science
on May 18, 1995, in partial fulfillment of the
requirements for the degree of
Master of Science in Electrical Engineering and Computer Science

Abstract

In deep space communications, arraying signals received at multiple ground antennas can be used to enhance communication downlink performance. By coherently adding signals received from the same spacecraft, arraying has the potential to increase the signal to noise ratio (SNR) over that achievable with any single antenna in the array. A number of different arraying techniques for use in NASA's Deep Space Network (DSN) have been proposed and their performance analyzed in past literature [1], [2]. These analyses have compared different arraying schemes under the assumption that the signals contain additive white Gaussian noise (AWGN), and that the noise observed at distinct antennas is independent.

In situations where an unwanted background body is visible to multiple antennas in the array, however, the assumption of independent noises is no longer applicable. A planet with significant radiation emissions in the frequency band of interest can be one such source of correlated noise. For example, during much of Galileo's tour of Jupiter, the planet will contribute significantly to the total system noise at various ground stations. This report analyzes the effects of correlated noise on two arraying schemes currently being considered for DSN applications; namely, full spectrum combining (FSC) and complex symbol combining (CSC). A framework is presented for characterizing the correlated noise based on physical parameters, and the impact of the noise correlation on the array performance is assessed for each scheme.

Thesis Supervisor: Robert Gallager
Title: Professor

Thesis Supervisor: Biren Shah
Title: Company Supervisor

Acknowledgments

The contributions of numerous individuals at the Jet Propulsion Laboratory to the work described in this thesis are gratefully acknowledged. I would like to thank Drs. David Rogstad and David Meier for their informative discussions on radio interferometry, Dr. Sami Hinedi for his insights on arraying techniques, Mr. Samson Million for his comments on software simulation methods, Dr. Victor Vilnrotter for his help in planning the radio interferometry experimeint, and Mr. Biren Shah and Dr. Mazen Shihabi for their advice in editing and organizing the thesis. In addition, I would like to thank my office mate, Dr. Ramin Sadr, for his continued encouragement and support in completing this thesis.

Contents

1 Introduction 9

2 Overview of Deep Space Communications and Telemetry Arraying 13

2.1 Signal Format and Single-Receiver Operation 13

2.2 Symbol SNR Degradation 16

2.3 FSC and CSC Arraying Techniques 18

2.3.1 Full Spectrum Combining 18

2.3.2 Complex Symbol Combining 21

2.3.3 Comparison of FSC and CSC 22

3 Modeling of Background Noise 25

3.1 Background Noise in a Single Receiver 25

3.2 Simple Radio Interferometer 27

3.3 Cross-correlation for Baseband Signals 32

3.4 Experimental Data 35

4 Full Spectrum Combining Performance 39

4.1 Ideal Arraying Gain 39

4.2 Symbol SNR Degradation 43

4.2.1 Antenna Phasing 44

4.2.2 Arrayed Symbol SNR and Symbol SNR Degradation 51

4.3 Simulation Results 53

5 Complex Symbol Combining Performance 57

5.1 Antenna phasing 58
5.2 Arrayed Symbol SNR and Symbol SNR Degradation 63
5.3 Simulation Results 65

6 Analysis of Full-Spectrum and Complex-Symbol Combining for Galileo Mission and Conclusion **69**
6.1 Galileo Signal Parameters 69
6.2 Arraying Performance 71
6.3 Conclusion 73

A Performance of the FSC Correlator **77**

B Performance of the CSC Correlator **81**

List of Figures

2-1 Spectrum of baseband telemetry signal 15

2-2 Single Receiver 15

2-3 Block diagram of full-spectrum combining 19

2-4 Block diagram of complex symbol combining 21

3-1 Spacecraft and background source in common beam 27

3-2 Antenna pair tracking distant source 28

3-3 Cross-correlation as a function of θ' 30

3-4 Fringe pattern against sky background 31

3-5 Experimental correlation data for 3C84 36

4-1 Ideal arraying gain G_A for various ρ, ψ 43

4-2 Conventional phase estimator 44

4-3 Complex correlation vector 45

4-4 Modified phase estimator 46

4-5 Phase estimate density 48

4-6 Phase estimate densities 49

4-7 Phase estimate densities 50

4-8 Phase estimate densities with simulation points 51

4-9 FSC degradation - theory and simulation 55

4-10 FSC degradation - theory and simulation 56

5-1 Matched filter noise outputs for CSC 67

5-2 CSC degradation - theory and simulation 68

5-3 CSC degradation - theory and simulation 68

6-1 Ideal arraying gain for Galileo signal, array of DSS-14 and DSS-15 . . 71

6-2 FSC performance for Galileo signal 72

6-3 CSC performance for Galileo signal 75

Chapter 1

Introduction

The process of combining radio signals from multiple antennas, commonly referred to as arraying, is becoming increasingly common in NASA's Deep Space Network (DSN) for spacecraft telemetry reception. By coherently adding signals from multiple receiving sites, arraying produces an enhancement in signal-to-noise ratio (SNR) over that achievable with any single antenna in the array. Arraying is especially attractive for deep space applications, since power constraints are typical in such communication systems. Arraying can be used to coherently demodulate signals that are too weak to be tracked by a single antenna, or to increase the supportable data rate for stronger signals, thereby increasing the scientific return from the mission.

A number of techniques for arraying spacecraft telemetry have been proposed and their performance analyzed in past literature [1], [2]. One performance measure discussed in these works for comparing arraying schemes is symbol SNR degradation. Degradation is defined as the ratio of the actual symbol SNR of the arrayed telemetry to that achievable with perfect synchronization (i.e., the "ideal" symbol SNR.) In general, synchronization losses result from imperfect combining of the signals, as well as phase errors in signal demodulation. Past work computed degradation for different arraying schemes under the assumption that the telemetry signals contain additive white Gaussian noise (AWGN), and that the noise waveforms from distinct antennas are independent.

In certain scenarios, an unwanted radio source within an antenna's reception pat-

tern can contribute significantly to total system noise. If such a background body is visible to multiple antennas in an array, the assumption of independent noises is no longer applicable. A planet with significant radiation emissions in the frequency band of interest can be one such source of correlated noise. For example, Jupiter is a strong radiator at S-band, which will be used for data return from the Galileo spacecraft. During a substantial fraction of the Galileo mission, the planet will have an angular separation from the spacecraft which is less than the beamwidth of a 70-meter antenna, which is the largest aperture antenna in the DSN. Further analysis is thus needed to characterize the performance of arraying schemes in the presence of correlated noise.

Prior work has been conducted on this subject, but has not exhausted research possibilities. A study by Dewey [3] examines correlated noise effects due to planetary sources, focusing mainly on physical considerations. A correlated noise model is presented, taking into account properties of the source and the array geometry. The impact of the background source on arrayed symbol SNR relative to the case of uncorrelated noise is then analyzed. The results obtained are applied to observation of the Galileo spacecraft from a 4-element array in the DSN's Australia complex. However, Dewey's study does not take into account the effects of imperfect synchronization in telemetry arraying, which are dependent on the specific arraying technique used. Thus, the analysis does not identify the relative advantages and disadvantages of different arraying schemes under conditions of correlated noise.

The purpose of this study is to analyze the effects of correlated noise on arraying, focusing on the processing scheme used. The full spectrum combining (FSC) and complex symbol combining (CSC) arraying techniques, which are presented in [2], are compared in terms of symbol SNR degradation. These schemes were chosen as the basis for this study because prior analysis indicates they are the most promising options when the link margin is low, as in the case of the Galileo S-band mission. Relative advantages and disadvantages of the two schemes will be identified, as well as the practical issue of modifications to existing techniques needed in the presence of correlated noise.

The body of this report is organized as follows: Chapter Two contains a tutorial introduction to deep space communications, and briefly introduces the full spectrum combining and complex symbol combining schemes. Chapter Three provides background information on radio sources, and presents an appropriate model for the noise observed by the antennas in an array. In Chapter Four, full spectrum combining is analyzed in detail, and simulation results of FSC performance with varying degrees of noise correlation are presented. Chapter Five contains the same analysis for the second scheme, complex symbol combining. Finally, Chapter Six applies the analysis of the previous three chapters to the case of the Galileo S-band mission and summarizes the major results of the work.

Chapter 2

Overview of Deep Space Communications and Telemetry Arraying

Here, we present basic information to familiarize the reader with deep space communications. Section 1 describes the deep space telemetry signal format, and explains the operation of a receiver needed to perform coherent symbol detection. In Section 2, symbol SNR degradation, which is a performance measure used to characterize both single-receiver and arrayed telemetry reception, is introduced. Section 3 provides a functional description of FSC and CSC, and briefly discusses their relative advantages and disadvantages.

2.1 Signal Format and Single-Receiver Operation

Deep space telemetry contains information in the form of binary data. A binary phase shift keyed (BPSK) modulation scheme with subcarrier is used; the ± 1 bit stream is directly modulated onto a squarewave subcarrier, which is then phase-modulated onto a carrier [1]. The received radio signal can thus be expressed as:

$$r(t) = \sqrt{2P_T}\cos(\omega_c t + \theta_c + \Delta d(t)\ \mathrm{sqr}(\omega_{sc} t + \theta_{sc})) + n(t) \qquad (2.1)$$

where P_T is the total received power; ω_c is the carrier radian frequency; Δ is the modulation index; d(t) is the ± 1 data stream; sqr(x) is the squarewave function, defined by sqr(x) = sgn(sin(x)); ω_{sc} is the subcarrier radian frequency; and n(t) is a bandpass white Gaussian noise process. Note that $n(t)$ consists of both noise due to front-end electronics of the receiving system, and noise due to any background sources in the antenna's field of view. A more detailed discussion of the background noise is given in Chapter 3. For now, we simply describe the total noise by its one-sided power spectral density level N_o.

The received radio signal is generally open-loop down-converted to some intermediate frequency before coherent demodulation takes place. In order to simplify the analysis, we will assume that all processing takes place at baseband. This represents no loss of generality, since the system performance should not depend on the frequency at which processing takes place. Coherent symbol detection at baseband requires down-conversion by two local oscillators in phase-quadrature. Using a trigonometric identity, the two baseband signals (commonly referred to as the "I" and "Q" components) can be expressed as

$$r_I(t) = \sqrt{P_C}\cos(\omega_b t + \theta_c) - \sqrt{P_D}d(t)\ \mathrm{sqr}(\omega_{sc}t + \theta_{sc})\sin(\omega_b t + \theta_c) + n_I(t) \quad (2.2)$$

$$r_Q(t) = \sqrt{P_C}\sin(\omega_b t + \theta_c) + \sqrt{P_D}d(t)\ \mathrm{sqr}(\omega_{sc}t + \theta_{sc})\cos(\omega_b t + \theta_c) + n_Q(t) \quad (2.3)$$

where ω_b is the baseband frequency (which, by definition, is close to zero); P_C is the carrier power, given by $P_C = P_T\cos^2\Delta$; P_D is the data power, given by $P_D = P_T\sin^2\Delta$; and $n_I(t)$ and $n_Q(t)$ are now lowpass Gaussian random processes. Note that the baseband noise processes each have spectral level N_o, and are independent. These signals can be represented more compactly as a single complex signal:

$$\tilde{r}(t) = \sqrt{P_C}\,e^{(j\omega_b t+\theta_c)} + j\sqrt{P_D}\,d(t)\ \ \mathrm{sqr}(\omega_{sc}t + \theta_{sc})e^{(j\omega_b t+\theta_c)} + \tilde{n}(t) \quad (2.4)$$

This complex notation will subsequently be used freely to represent a pair of baseband signals. The spectrum of the baseband signal $\tilde{r}(t)$ is shown in Figure 2-1. Note that

the signal consists of a residual carrier tone at frequency $f_b = 2\pi\omega_b$, surrounded by data sidebands spaced at odd multiples of the subcarrier frequency $f_{sc} = 2\pi\omega_{sc}$.

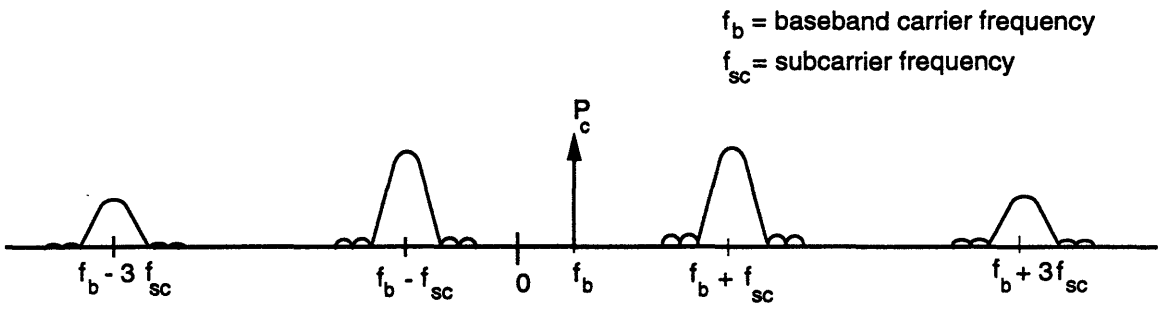

Figure 2-1: Spectrum of baseband telemetry signal

Symbol detection requires coherent carrier and subcarrier tracking, as well as symbol synchronization to drive the matched filter output. A block diagram of a single receiver is shown in Figure 2-2. The operation of each of these blocks is easily illustrated by use of equations. Assume for the moment that perfect carrier, subcarrier and symbol references are available. After carrier demodulation, the signal is given by

$$\begin{aligned} \tilde{u}(t) &= \tilde{r}(t)\, e^{-j(\omega_b t+\theta_c)} \\ &= \sqrt{P_C} + j\sqrt{P_D}\, d(t)\ \ \mathrm{sqr}(\omega_{sc}t + \theta_{sc}) + \tilde{n}'(t) \end{aligned} \tag{2.5}$$

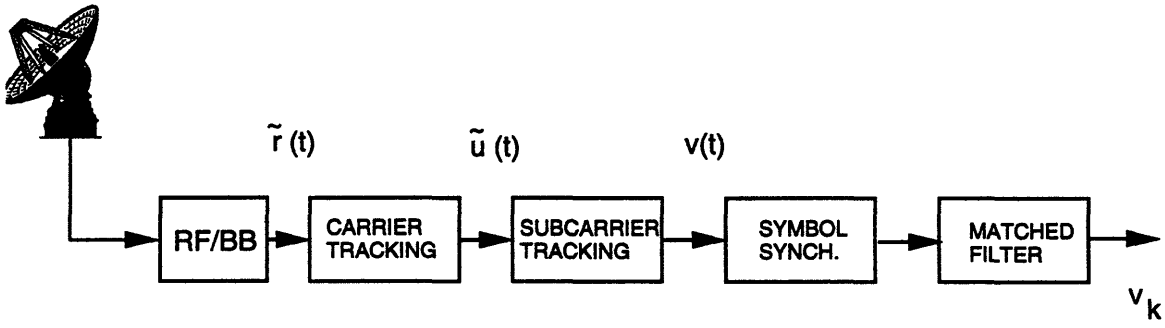

Figure 2-2: Single Receiver

The data is contained solely in the imaginary part of the signal $\tilde{u}(t)$. Multiplying

this by the ideal subcarrier reference then yields the data stream alone, i.e.,

$$\begin{aligned} v(t) &= \mathrm{Im}[\tilde{u}(t)]\ \ \mathrm{sqr}(\omega_{sc}t + \theta_{sc}) \\ &= \sqrt{P_D}d(t) + n'(t) \end{aligned} \tag{2.6}$$

Finally, the symbol synchronizer provides timing for the matched filter, whose output is given by

$$\begin{aligned} v_k &= \frac{1}{T_s}\int_{kT_s}^{(k+1)T_s} v(t) \\ &= \sqrt{P_D}d_k + n_k \end{aligned} \tag{2.7}$$

where k denotes the symbol index, and T_s is the symbol duration. Note that the noise output of the matched filter has variance $\frac{N_o}{2T_s}$. The symbol SNR is defined as the mean of the matched filter output squared divided by its variance, and is equal to $2P_DT_s/N_o$ in the case where ideal references are available.

2.2 Symbol SNR Degradation

In practice, perfect references for all three stages of synchronization are not available. Carrier and subcarrier tracking loops are used to perform the demodulation, and a symbol synchronization loop is used to obtain symbol timing. Synchronization errors in each of these three loops thus result in an SNR at the matched filter output which is less than the ideal case. Symbol SNR degradation is defined as the ratio of the actual achieved symbol SNR to the ideal symbol SNR, and is used as a measure of receiver performance. A quantitative evaluation of degradation for a single receiver is given in [1], and the main results are summarized here.

In the presence of phase errors in each of the three loops, the matched filter output is given by

$$v_k = \sqrt{P_D}\, d_k(\cos\phi_c)\,(1 - \frac{2}{\pi}|\phi_{sc}|)\,(1 - \frac{1}{2\pi}|\phi_{sy}|) + n_k$$

$$= \sqrt{P_d} d_k \, C_c \, C_{sc} \, C_{sy} + n_k \tag{2.8}$$

where $\phi_c, \phi_{sc}, \phi_{sy}$ are the carrier, subcarrier, and symbol phase errors in radians, respectively, and the C factors are the signal reduction functions for each of the three loops. Note that the total signal reduction function can be factored into three separate terms, but the three phase errors are, in general, non-independent. The symbol SNR conditioned on the phase errors of the three loops is then given by

$$SNR' = \frac{2P_d T_s}{N_o} C_c^2 C_{sc}^2 C_{sy}^2 \tag{2.9}$$

The unconditional SNR is found by taking the expectation of (2.9) with respect to the various phase errors. The tracking performance of each of the three loops is a function of its respective *loop SNR*, which is defined as the inverse of the steady-state phase error variance. The loop SNRs for the carrier, subcarrier, and symbol loops are respectively given by

$$\rho_c = \frac{P_D}{N_o B_c} \left(1 + \frac{1}{2E_s/N_o}\right)^{-1} \tag{2.10}$$

$$\rho_{sc} = \left(\frac{2}{\pi}\right)^2 \frac{P_D/N_o}{B_{sc} W_{sc}} \left(1 + \frac{1}{2E_s/N_o}\right)^{-1} \tag{2.11}$$

$$\rho_{sy} = \frac{P_D/N_o}{2\pi^2 W_{sy} B_{sy}} \frac{\left(\mathrm{Erf}\left(\sqrt{\frac{E_s}{N_o}}\right) - \frac{W_{sy}}{2\sqrt{\pi}} \sqrt{\frac{E_s}{N_o}} e^{-E_s/N_o}\right)}{\left(1 + \frac{E_s}{N_o}\frac{W_{sy}}{2} - \frac{W_{sy}}{2}\left[\frac{1}{\sqrt{\pi}} e^{-E_s/N_o} + \sqrt{\frac{E_s}{N_o}} \mathrm{Erf}\left(\sqrt{\frac{E_s}{N_o}}\right)\right]^2\right)} \tag{2.12}$$

where B_c, B_{sc}, and B_{sy} are the carrier, subcarrier, and symbol loop bandwidths, respectively; W_{sc} and W_{sy} are the subcarrier and symbol windows; E_s is the symbol energy, given by $E_s = P_D T_S$; and $\mathrm{Erf}(x)$ is the error function, given by $\mathrm{Erf}(x) = 2/\sqrt{\pi} \int_0^x e^{-w^2} dw$. In expressing ρ_c, it has been assumed that a Costas loop is used for carrier tracking. The second moments of the reduction functions are related to the loop SNRs by the following:

$$\overline{C_c^2} = \frac{1}{2}\left[1 + \frac{I_2(\frac{1}{4}\rho_c)}{I_0(\frac{1}{4}\rho_c)}\right] \tag{2.13}$$

$$\overline{C_{sc}^2} = 1 - \frac{4}{\pi}\sqrt{\frac{2}{\pi\rho_{sc}}} + \frac{4}{\pi^2}\frac{1}{\rho_{sc}} \tag{2.14}$$

$$\overline{C_{sy}^2} = 1 - \frac{1}{\pi}\sqrt{\frac{2}{\pi\rho_{sy}}} + \frac{1}{4\pi^2}\frac{1}{\rho_{sy}} \tag{2.15}$$

where $\overline{x}$ denotes expectation of x, and $I_k(x)$ denote the modified Bessel function of order k. The first moments of the subcarrier and symbol reduction functions will be needed in later analysis, and are given by

$$\overline{C_{sc}} = 1 - \frac{2}{\pi}\sqrt{\frac{2}{\pi\rho_{sc}}} \tag{2.16}$$

$$\overline{C_{sy}} = 1 - \frac{1}{2\pi}\sqrt{\frac{2}{\pi\rho_{sy}}} \tag{2.17}$$

Thus, the degradation for a single receiver is given by

$$D = \overline{C_c^2}\,\overline{C_{sc}^2}\,\overline{C_{sy}^2} \tag{2.18}$$

where $\overline{C_c^2}, \overline{C_{sc}^2}$, and $\overline{C_{sy}^2}$ are found by combining (2.10) - (2.12) with (2.13) - (2.15).

2.3 FSC and CSC Arraying Techniques

We now provide a brief introduction to the full-spectrum combining and complex symbol combining arraying schemes, which are described in detail in [2]. Each of these techniques will be treated in more depth in subsequent chapters; here, we merely provide a functional overview to illustrate the basic concept of arraying, and to point out the main differences between the two schemes.

2.3.1 Full Spectrum Combining

Full-spectrum combining is conceptually the more simple of the two schemes being considered. A block diagram of FSC for an array of L antennas is shown in Figure 2-3. Following down-conversion to baseband, each signal is delayed by some amount τ_i to compensate for differing arrival times of the spacecraft signal at each antenna.

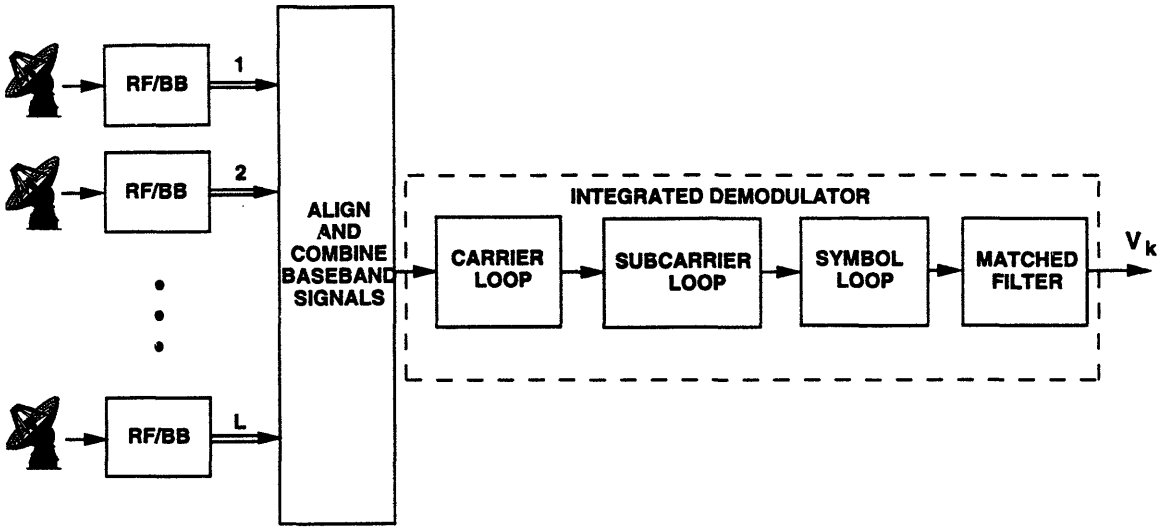

Figure 2-3: Block diagram of full-spectrum combining

The quantities τ_i can typically be computed in advance from the spacecraft trajectory and automatically adjusted over the course of a tracking pass. The delayed baseband signal from the i^{th} antenna is given by

$$\tilde{r}_i(t) = \sqrt{P_{C_i}}\, e^{(j\omega_b t + \theta_{c_i})} + j\sqrt{P_{D_i}}\, d(t)\ \ \mathrm{sqr}(\omega_{sc} t + \theta_{sc}) e^{(j\omega_b t + \theta_{c_i})} + \tilde{n}_i(t) \qquad (2.19)$$

Note that the signals are aligned in time, but that the carrier phases θ_{c_i} are not necessarily the same. Before the signals may be added coherently, $L-1$ of the signals must be phase-rotated. We will designate antenna 1 as the reference antenna, such that $\tilde{r}_i(t)$ must be rotated by an amount $\phi_{1i} \triangleq \theta_{c_1} - \theta_{c_i}$ for $i = 2 \ldots L$. Estimates of the relative phases, $\hat{\phi}_{1i}$, are computed in real time by correlating each signal with $\tilde{r}_1(t)$. Note that the combining block and the carrier loop perform distinct but related functions: the former compensates for the differential phase between the various signal pairs, while the latter tracks the component of the phase common to all the signals.

For now, assume the desired phases ϕ_{1i} are estimated perfectly. Each signal is phase-rotated by the appropriate amount and multiplied by some pre-specified weight

β_i, and the resulting signals are summed coherently, i.e.,

$$\tilde{r}_{comb}(t) = \sum_{i=1}^{L} \beta_i \, \tilde{r}_i(t) \, e^{j\phi_{1i}} \tag{2.20}$$

$$= e^{j(\omega_b t+\theta_1)} \sum_{i=1}^{L} \beta_i \left(\sqrt{P_{C_i}} + j\sqrt{P_{D_i}} \, d(t) \, \mathrm{sqr}(\omega_{sc} t + \theta_{sc}) \right) + \sum_{i=1}^{L} \beta_i \tilde{n}_i(t) \, e^{j\phi_{1i}} \tag{2.21}$$

Finally, the combined signal is tracked by one carrier, subcarrier, and symbol loop, yielding an arrayed symbol stream given by

$$v_{k_{comb}} = \sum_{i=1}^{L} \beta_i \sqrt{P_{D_i}} \, d_k + \sum_{i=1}^{L} \beta_i \, n_{k_i} \tag{2.22}$$

where we have assumed perfect synchronization at each of the three stages. It is shown in [1] that when the noises from distinct antennas are independent, the SNR of the above expression is maximized if the weighting factors are chosen to satisfy the condition

$$\beta_i = \sqrt{\frac{P_{D_i}}{P_{D_1}} \frac{N_{o_1}}{N_{o_i}}} \tag{2.23}$$

in which case the ideal combined SNR becomes

$$SNR_{comb} = \frac{2P_{D_1}T_s}{N_{o_1}} \sum_{i=1}^{L} \gamma_i \tag{2.24}$$

$$= \frac{2P_{D_1}T_s}{N_{o_1}} G_A \tag{2.25}$$

where $\gamma_i \triangleq \frac{P_{D_i}}{P_{D_1}} \frac{N_{o_1}}{N_{o_i}}$. The factor G_A is known as the *arraying gain.* Typically, antenna 1 is specified to be the antenna with the strongest signal (i.e., the highest P_T/N_o). The arraying gain then describes the increase in SNR over that achievable with any single antenna in the array. For the case of uncorrelated noises, we see that the effective $\frac{P_D}{N_o}$ of the combined signal is equal to the *sum* of the $\frac{P_D}{N_o}$'s of the individual antennas.

2.3.2 Complex Symbol Combining

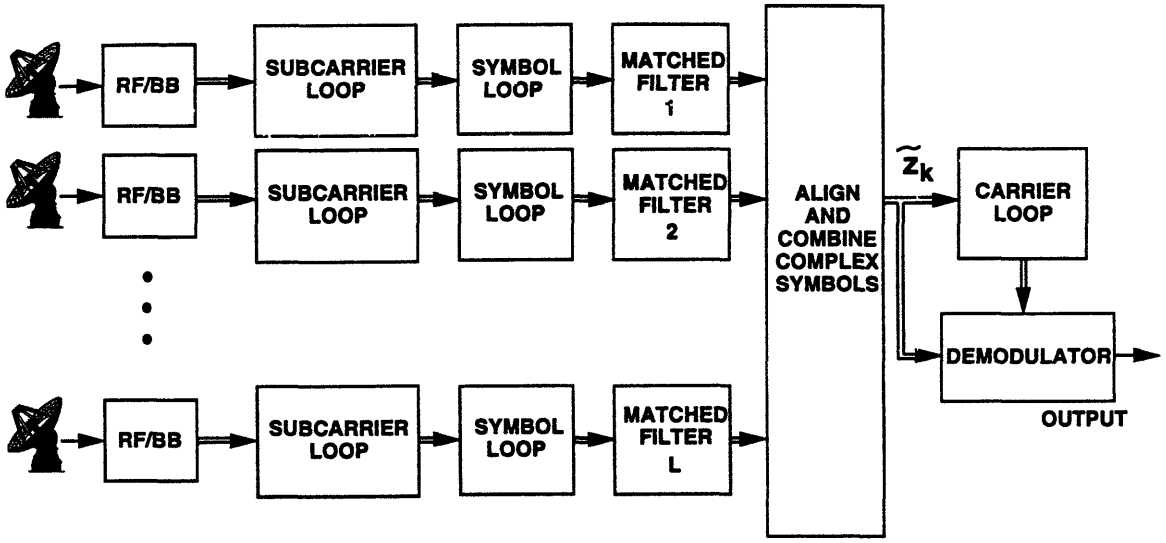

Figure 2-4: Block diagram of complex symbol combining

A block diagram of complex symbol combining for an L antenna array is shown in Figure 2-4. Here, the baseband signals are tracked by separate subcarrier and symbol loops *before* the carrier is coherently demodulated. Thus, the baseband signal from the i^{th} antenna is first multiplied by the subcarrier reference from the i^{th} subcarrier loop, i.e.,

$$\tilde{u}_i(t) = \tilde{r}_i(t)\ \mathrm{sqr}(\omega_{sc}t + \theta_{sc}) \tag{2.26}$$

$$= \sqrt{P_{C_i}}\, e^{(j\omega_b t + \theta_{c_i})}\ \mathrm{sqr}(\omega_{sc}t + \theta_{sc}) + j\sqrt{P_{D_i}}\, d(t)\, e^{(j\omega_b t + \theta_{c_i})} + \tilde{n}'(t) \tag{2.27}$$

where, once again, we have assumed perfect subcarrier reference for simplicity. This signal is then passed through a matched filter, whose timing is obtained from the i^{th} symbol loop, yielding a carrier-modulated symbol stream given by

$$\tilde{z}_{k_i} = \sqrt{P_{D_i}}\, e^{j(\omega_b k T_s + \theta_{c_i})}\, d_k + n_{k_i} \tag{2.28}$$

where we have implicitly assumed that the carrier phase is nearly constant over one symbol interval (i.e., $f_b T_s \ll 1$). Note that the residual carrier term, $\sqrt{P_{C_i}}\, e^{(j\omega_b t + \theta_{c_i})}$,

multiplied by the subcarrier reference integrates to zero.

These complex baseband symbols are then transmitted to a central location where they are phase-aligned, weighted, and combined, as in the case of full spectrum combining. The combined signal is thus given by

$$\tilde{z}_{k_{comb}} = e^{j(\omega_b k T_s + \theta_{c_1})} \sum_{i=1}^{L} \beta_i \sqrt{P_{D_i}}\, d_k + \sum_{i=1}^{L} \beta_i\, n'_{k_i} \tag{2.29}$$

A baseband Costas loop is finally used to demodulate the carrier, and the arrayed symbol stream is given by

$$v_{k_{comb}} = \sum_{i=1}^{L} \beta_i \sqrt{P_{D_i}}\, d_k + \sum_{i=1}^{L} \beta_i\, n''_{k_i} \tag{2.30}$$

Once again, when the noise at separate antennas is independent, the SNR of (2.30) is maximized by setting the weighting factors according to (2.23). The ideal SNR of the arrayed telemetry is then given by (2.25).

2.3.3 Comparison of FSC and CSC

We have seen that the "ideal" symbol SNR is the same for full spectrum combining and complex symbol combining in the absence of correlated noise. This result follows from intuition; if demodulation and combining can be achieved perfectly, it should not matter in which order the various processes take place. The same reasoning holds for the correlated noise case: the ideal symbol SNR will be different from (2.25), but will be independent of which scheme is used.

The performance of the two techniques will, however, be different when synchronization losses are accounted for. Note that when telemetry is arrayed, synchronization losses arise from imperfect carrier, subcarrier, and symbol tracking, as well as errors in phase-aligning the signals. In full-spectrum combining, the loop SNRs of each of the carrier, subcarrier, and symbol loops are increased by arraying the signals. By contrast, only the carrier loop SNR enjoys the benefit of the arraying gain in complex symbol combining. In addition, the subcarrier and symbol loops must operate

in the absence of carrier lock for CSC, resulting in a further reduction in loop SNR[1]. Thus, losses due to subcarrier and symbol tracking are higher for complex symbol combining than for full spectrum combining. Differences in the method of combining similarly lead to different synchronization losses.

Symbol SNR degradation is used as a measure of relative performance for the two schemes. Similar to the case of a single receiver, degradation is defined as the ratio of the actual to ideal *arrayed* symbol SNR. Degradation for each of these arraying schemes has been analyzed in past literature for the case where the noise encountered at the various antennas are independent [2]. We will later extend this analysis to include the case of arbitrary noise correlation between the various antennas.

We note that the effects of correlated noise on arraying can be separated into two different but related factors. The first is the ideal arraying gain, which will be dependent on the correlation properties of the noise itself, but independent of which scheme is used. The second is the degradation, which will depend on the noise properties *as well* as which arraying technique is used. Each of these will be analyzed in turn in Chapters 4 and 5; we presently turn to a discussion of radio sources to develop an appropriate model for correlated noise due to a common background.

[1]Modified subcarrier and symbol loops have been developed for use with complex symbol combining. These loops utilize information in both the I and Q components of the complex signal to recover some of the loss in loop SNR due to the absence of carrier lock. The relevant details will be presented in Chapter 5, where CSC is analyzed in further detail.

Chapter 3

Modeling of Background Noise

This chapter covers basic concepts needed to characterize noise due to radio sources. The first section presents terminology used in radio science to describe broadband sources, and shows how the effect of background noise on a single receiving system can be accounted for by an equivalent *source temperature.* In the second section, we consider the effect of a noisy background on a pair of antennas, using interferometry theory to compute the cross-correlation function of the received noise waveforms. Section three extends this analysis to a baseband receiving system, which will be assumed for the remainder of this work. Finally, section four presents the results of an experiment that was conducted to illustrate the basic principles outlined in this chapter.

3.1 Background Noise in a Single Receiver

In deep space communications, signals are generally assumed to be received through an additive white Gaussian noise channel. The noise level in a receiving system is commonly characterized by a system temperature, T_{sys}. The one-sided power spectral density of the noise is then given by $N_o = kT_{sys}$, where k is Boltzmann's constant. Background sources such as planets are typically broad-band, and have an emission spectrum that is reasonably flat over a frequency range of interest. Receiving bandwidths for deep space applications are typically no greater than 100 MHz, over which

the background noise can essentially be considered white. Thus, the noise level contributed by the background can be described by a background temperature, T_b, which measures the contribution of the source to the total system noise. Here, we show how this temperature can be computed from more physically informative characteristics of the source.

A radio source is generally described by its *brightness distribution*, $B(\phi, \theta)$, which has units of $W/m^2/Hz/sr$ [1]. The variables ϕ and θ indicate that brightness refers to a particular direction; an arbitrary source may have some parts that radiate more strongly than others. The total strength of the source can be measured by its *flux density*, S, which is equal to the brightness distribution integrated over the angular extent of the source, i.e.,

$$S = \int \int B(\phi, \theta) d\Omega \tag{3.1}$$

where the integration variable Ω denotes integration over a solid angle. Thus, the units of flux density are $W/m^2/Hz$. Note that the flux density of a particular source depends on its distance from Earth; the closer the source, the larger solid angle it subtends, and hence the larger the flux density becomes.

The noise level due to such a source as observed by a receiving antenna can be described by a background temperature, as discussed above, which is given by

$$T_b = \frac{A_e}{2k} \int \int B(\phi, \theta) P_N(\phi, \theta) d\Omega \tag{3.2}$$

where A_e is the effective collecting area of the antenna, and $P_N(\phi, \theta)$ is the normalized antenna reception pattern. Thus, the contribution of a background source to total system noise depends on the strength of the source and its position in the antenna pattern. For telemetry applications, the antenna is pointed at the spacecraft, so the contribution of a given source varies with its angular separation from the spacecraft. This situation is depicted in Figure 3-1.

In the worst-case scenario, the source-to-spacecraft angular separation is zero or

[1] The unit *sr* stands for steradian, which is a measure of solid angle.

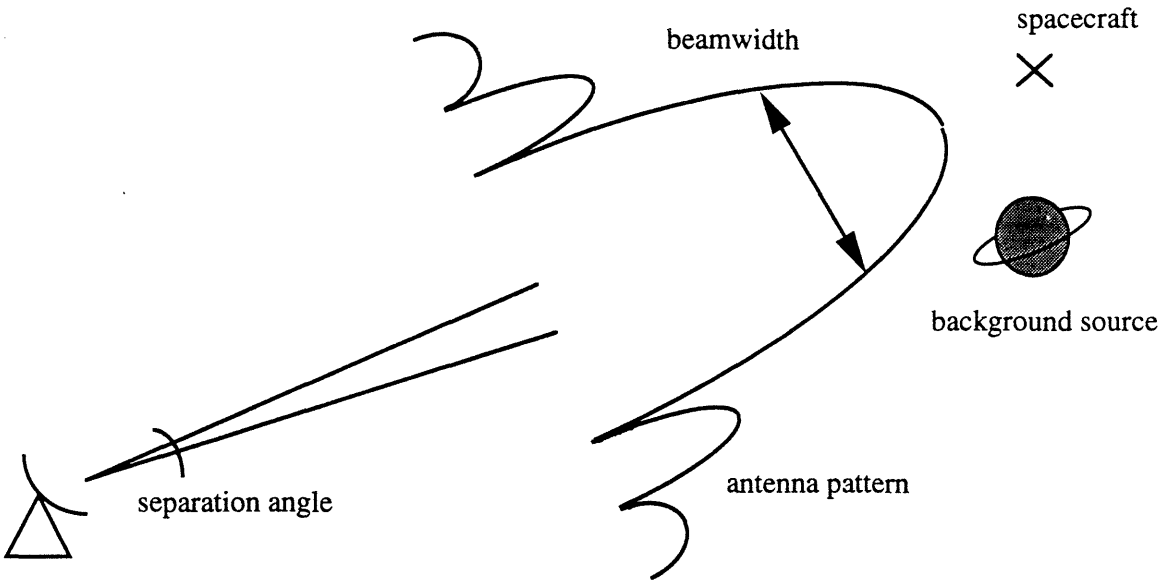

Figure 3-1: Spacecraft and background source in common beam

negligibly small compared to the beamwidth of the antenna. The antenna pattern term, P_N, then approaches unity over the integral, and

$$T_b = \frac{A_e}{2k} \int \int B(\phi, \theta) d\Omega \tag{3.3}$$

$$= \frac{A_e}{2k} S \tag{3.4}$$

An upper limit on the total system temperature that a source can contribute can thus be computed from the flux density of the source and the effective area of the receiving antenna.

3.2 Simple Radio Interferometer

We now turn to the properties of correlated background noise as observed by two antennas. Specifically, this section computes the cross-correlation function of the noise due to the source. A pair of antennas basically behaves as an interferometer, and computation of the cross-correlation function follows from fundamental principles of interferometry. We start by considering an oversimplified model for illustrative

purposes, and then gradually move to one that more accurately describes an actual receiving system. The discussion below provides a general idea of the issues involved, and is not meant to be a rigorous treatment of the subject. A more thorough analysis can be found in a text on radio astronomy, such as [6].

Consider two antennas tracking a distant radio source, as depicted in Figure 3-2. The received noise waveforms are filtered by some front-end filter centered at

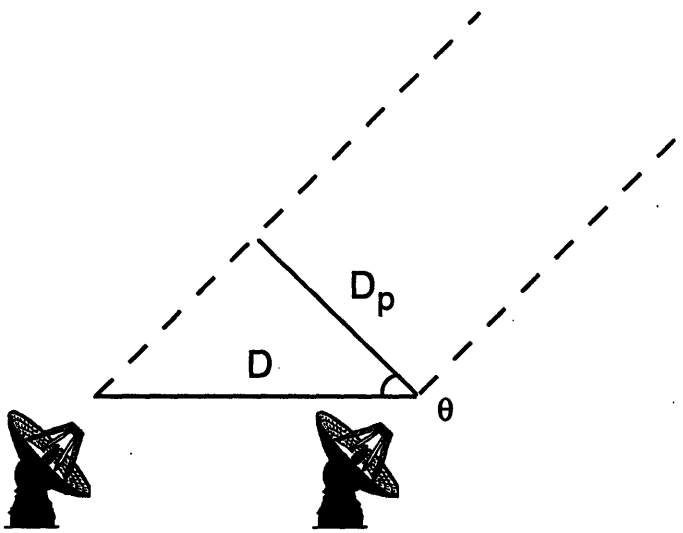

Figure 3-2: Antenna pair tracking distant source

frequency f_o. Since the received noise is white, the form of the correlation function is determined solely by the characteristics of the front-end filters. The cross-correlation function of the noise waveforms is defined as

$$R(\tau) = E[n_1(t)n_2(t-\tau)] \tag{3.5}$$

Note that $n_1(t)$ and $n_2(t)$ can be taken to be the noises due to the background source alone or the total noise waveforms at antennas 1 and 2, since the noises due to front-end electronics are independent. In the case of a simple point source, the received waveforms are identical except for some geometric delay τ_g. The cross-correlation function then takes the form

$$R(\tau) = G(\tau - \tau_g)\cos 2\pi f_0(\tau - \tau_g) \tag{3.6}$$

where $G(\tau)$ is some function determined by the shape of the front-end filters. For example, in the case of a rectangular passband of one-sided bandwidth B, $G(t)$ would be given by $\sin \pi Bt/\pi t$. Under typical conditions, the receiving bandwidth is much smaller than the center frequency. Thus, the correlation function consists of a slowly-varying envelope modulated by a rapidly-varying sinusoid at the center frequency of the passband. The latter is referred to as the *delay pattern*, while the former is known as the *fringe pattern.*

The geometric delay is due to the difference in path lengths from the source to each of the two antennas. From Figure 5, it is readily seen that τ_g can be expressed as

$$\tau_g = \frac{D \sin \theta}{c} \tag{3.7}$$

where D is the separation baseline between the two antennas in meters, θ is the angle as shown in Figure 5, and c is the speed of light. The correlation function thus has both a temporal and spatial dependence. To consider the effect of varying the angle θ, the above quantity can be expanded in a first-order Taylor series about some reference position θ_0:

$$\tau_g \approx \frac{D}{c}(\sin \theta_0 + \theta' \cos \theta_0) \tag{3.8}$$

where $\theta = \theta_0 + \theta'$. Now let one of the signals be delayed by some amount τ_{g0} equal to the geometric delay at angle θ_0. Inserting (3.8) into the shifted cross-correlation function yields

$$R(\tau, \theta') = G(\tau - \frac{D}{c}\theta' \cos \theta_0) \cos 2\pi f_0 (\tau - \frac{D}{c}\theta' \cos \theta_0) \tag{3.9}$$

This function is plotted as a function of θ' for a fixed value of τ in Figure 3-3. Note that the quantity $D_p = D \cos \theta_0$ is the projected baseline in the direction of the source. (See Figure 3-2) The spacing between the oscillations is given by $w = c/(f_o D_p)$. This quantity, known as the fringe spacing, has important implications for the measured noise correlation due to an arbitrary source. Recall that the expression given in (3.9) was developed for a point source. In general, the correlation function due to a source of non-infinitesimal size will have to be computed as an integral of the above

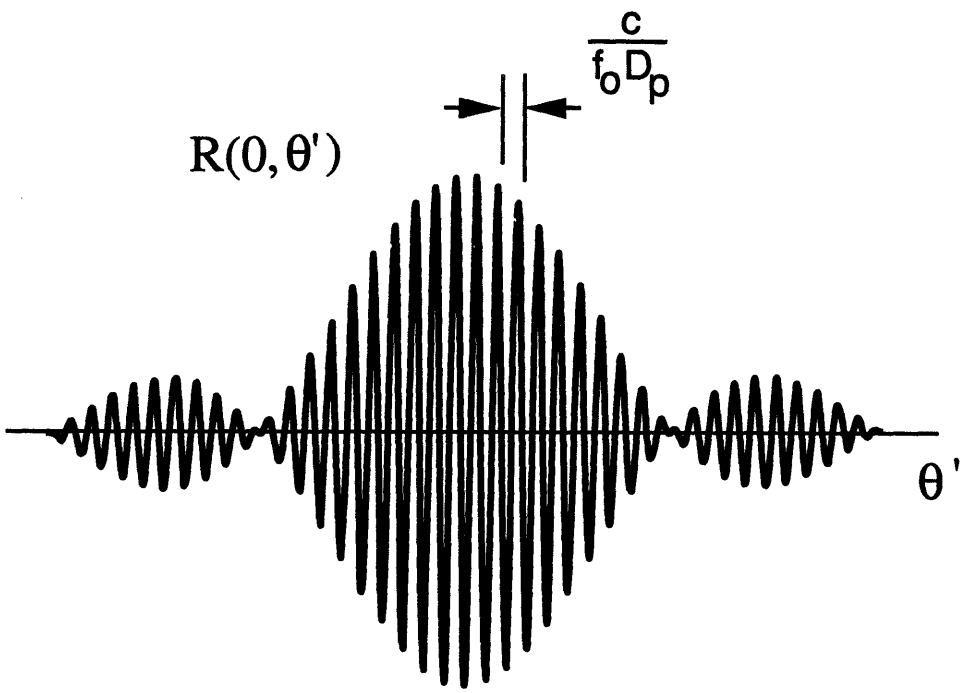

Figure 3-3: Cross-correlation as a function of θ'

expression over the angular extent of the body. If the body being observed subtends many fringe cycles, then the measured correlation tends to zero due to the averaging effect of the sinusoid. Such a body is said to be *resolved* by the array.

Figure 3-4 shows the interference pattern formed by two antennas against a sky background. Here, it can be seen that the angular size of the source relative to the fringe spacing is what determines whether or not the source is resolved by the array. For a given source and observation frequency, the length of the baseline determines the degree to which the source is resolved. Consider a source having an angular radius of R_s radians observed at some frequency f_o Hz. In the long baseline limit, where $D_p \gg c/(f_o R_s)$, the fringe spacing is extremely small compared to the size of the source, and the noise correlation tends to zero. By contrast, for extremely short baselines, such that $D_p \ll c/(f_o R_s)$, the effect of the averaging sinusoid is negligible, and the noise correlation is maximized. Thus, the degree of noise correlation observed depends heavily on the geometry of the array. This point is stressed in [3], where it is stated that the more compact the array configuration, the greater the impact of the background body on the array. As an example, consider observing Jupiter at S-band

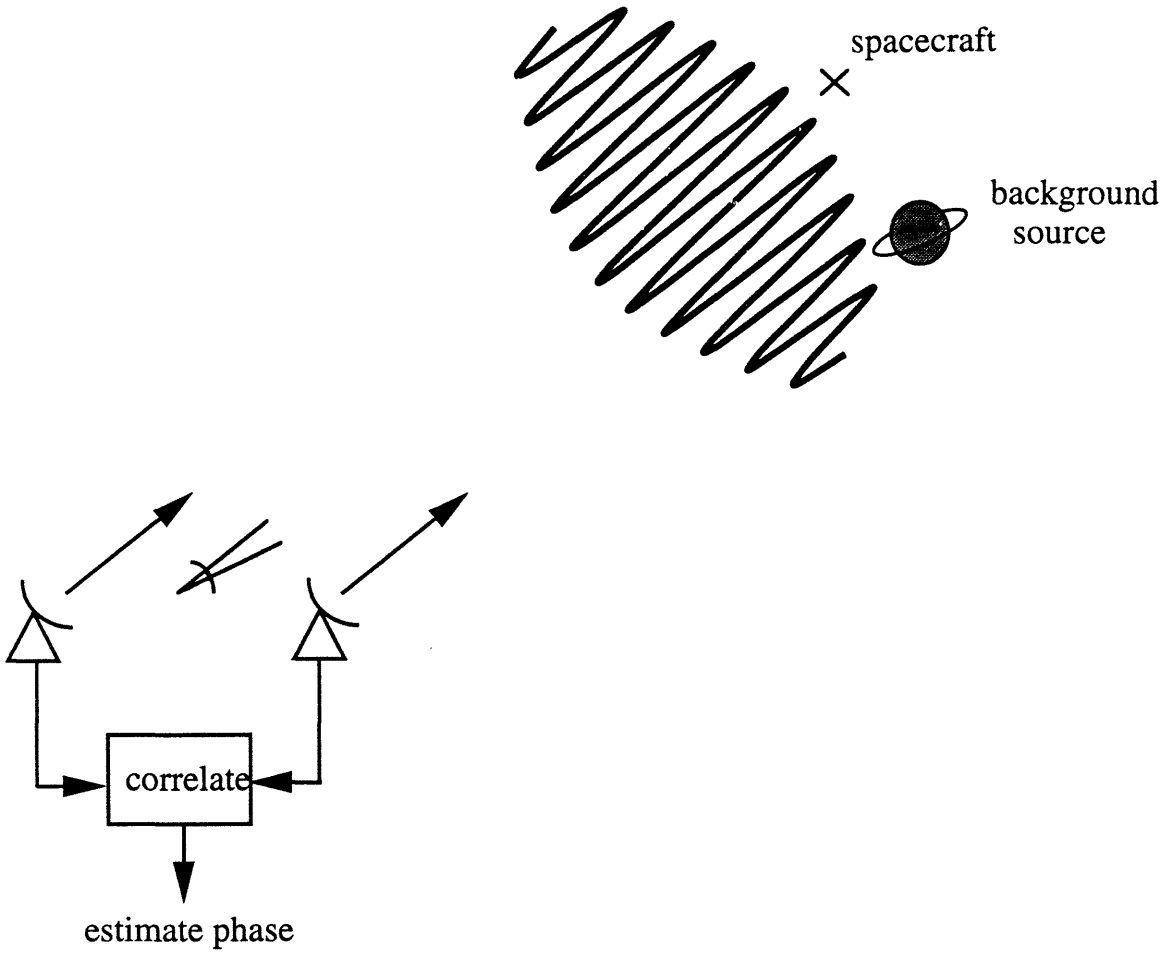

Figure 3-4: Fringe pattern against sky background

(2.3 GHz). The planet's angular size varies with its distance to earth, but a typical value is 10^{-3} radians. An antenna separation on the order of a few hundred meters would thus be required to observe a measurable degree of noise correlation.

At this point, a more general expression for the cross-correlation for an arbitrary source can be presented. It is shown in [6] that $R(\tau)$ can be expressed as

$$R(\tau) = G(\tau)\frac{\sqrt{A_{e_i}A_{e_k}}}{2}\int\int\sqrt{P_{N_i}(\sigma)P_{N_k}(\sigma)}B(\sigma)\cos 2\pi f_o(\tau - \vec{B}_{ik}\cdot\sigma/c)d\Omega \quad (3.10)$$

where σ is a unit vector specifying the direction, $P_{N_i}(\sigma)$ and $P_{N_k}(\sigma)$ are the normalized

antenna reception patterns in the direction σ, A_{e_i} and A_{e_k} are the effective areas of the two antennas, $B(\sigma)$ is the brightness of the source in the direction σ, $\vec{B_{ik}}$ is the baseline vector, and $d\Omega$ is the element of solid angle over which the integral is taken. Note that the effect of spatial variations on the delay pattern term, G, has been neglected. This approximation is justified if the received signals are narrowband, since the delay term then varies much more slowly than the fringe term. This can be seen graphically in Figure 3-4; over the integral, the envelope of the interferometer reception pattern is essentially constant, while the sinusoidal component is more quickly-varying. In addition, it has been assumed that the correct geometric delay has been inserted to compensate for the differential pathlength to the source.

A useful quantity known as the *complex visibility* can be defined as

$$V = |V|e^{j\phi_v} = \int\int \sqrt{P_{N_i}(\sigma)P_{N_k}(\sigma)}B(\sigma)e^{-j2\pi\vec{B}_{ik}\cdot\sigma/c}\, d\Omega \tag{3.11}$$

After some manipulation, $R(\tau)$ can be expressed as

$$\begin{aligned} R(\tau) &= \frac{\sqrt{A_{e_i}A_{e_k}}}{2}G(\tau)|V|\cos(2\pi f_o\tau - \phi_v) && (3.12)\\ &= \alpha G(\tau)\cos(2\pi f_o\tau - \phi_v) && (3.13)\end{aligned}$$

where A_{e1} and A_{e2} are the effective collecting areas of the two antennas. The variable $\alpha = \frac{\sqrt{A_{e1}A_{e2}}}{2}|V|$ has been introduced for notational convenience, and is the cross power spectral density between the two noise waveforms, having units of W/Hz. Note that V has the same units as flux density (W / m^2 / Hz). In the upper limit, all terms in the integrand of (3.11) except the source brightness approach unity, and V approaches the flux density of the source being observed.

3.3 Cross-correlation for Baseband Signals

As discussed in Chapter 2, we are assuming that all processing takes place at baseband. Thus, here we compute the cross-correlation for the equivalent baseband sig-

nals. Recall that each bandpass RF signal is down-converted by two oscillators in phase quadrature, resulting in a pair of baseband signals. Consider representing the bandpass signals as

$$\begin{aligned} n_1(t) &= x_1(t)\cos\omega_o t - y_1(t)\sin\omega_o t \\ n_2(t) &= x_2(t)\cos\omega_o t - y_2(t)\sin\omega_o t \end{aligned} \tag{3.14}$$

where $\omega_o = 2\pi f_o$. Let $n_1(t)$ and $n_2(t)$ be bandpass Gaussian random processes centered in frequency at f_o, and having spectral levels N_{o1} and N_{o2}, respectively. It is shown in [4] that $x_i(t)$ and $y_i(t)$ are then lowpass Gaussian random processes with spectral levels $2N_{o_i}$, and that $x_i(t)$ and $y_i(t)$ are uncorrelated for all t $(i = 1, 2)$. Expressing the cross-correlation function in terms of these lowpass processes, we find

$$\begin{aligned} R_{n1,n2}(\tau) &= E[n_1(t)n_2(t-\tau)] \\ &= \frac{1}{2}(R_{x1,x2}(\tau) + R_{y1,y2}(\tau))\cos\omega_o\tau + \frac{1}{2}(R_{x1,x2}(\tau) - R_{y1,y2}(\tau))\cos(2\omega_o t - \omega_o\tau) \\ &+ \frac{1}{2}(R_{y1,x2}(\tau) - R_{x1,y2}(\tau))\sin\omega_o\tau - \frac{1}{2}(R_{y1,x2}(\tau) + R_{x1,y2}(\tau))\sin(2\omega_o t - \omega_o\tau) \end{aligned} \tag{3.15}$$

This can now be related to the form of the cross-correlation function found from section 2. Assuming the fixed delay is not inserted, we know $R_{n1,n2}$ takes the form

$$\begin{aligned} R_{n1,n2}(\tau) &= \alpha G(\tau - \tau_g)\cos(\omega_o\tau - \phi_v) \\ &= \alpha G(\tau - \tau_g)\cos\phi_v\,\cos\omega_o\tau + \alpha G(\tau - \tau_g)\sin\phi_v\,\sin\omega_o\tau \end{aligned} \tag{3.16}$$

Thus, the equivalence between (3.15) and (3.16) holds only if the following symmetry conditions are true:

$$\begin{aligned} R_{x1,x2}(\tau) &= R_{y1,y2}(\tau) = \alpha G(\tau - \tau_g)\cos\phi_v \\ R_{y1,x2}(\tau) &= -R_{x1,y2}(\tau) = \alpha G(\tau - \tau_g)\sin\phi_v \end{aligned} \tag{3.17}$$

At this point, it is straightforward to show that the cross-correlation of the complex baseband signals will take a similar form:

$$R_{\tilde{n}1,\tilde{n}2}(\tau) = E[\tilde{n}_1(t)\tilde{n}_2^*(t-\tau)] = \alpha G(\tau - \tau_g)e^{j\phi_{12}^n} \tag{3.18}$$

The phase ϕ_{12}^n accounts for the visibility phase ϕ_v plus any phase difference introduced by the local oscillators at the two antennas. After down-conversion to baseband, one of the complex signals is delayed by an amount τ_{g_o} to compensate for the geometric delay at some position θ_o. In practice, this delay is computed based on the position of the spacecraft. This delay will, in general, be different from the quantity τ_g in (3.18), since the background source is at a slightly different position than the spacecraft. However, we will assume that this "residual delay" is very small compared to the inverse filter-bandwidth. Thus, (3.18) becomes

$$R_{\tilde{n}_1,\tilde{n}_2}(\tau) \approx \alpha G(\tau)e^{j\phi_{12}^n} \tag{3.19}$$

where $G(\tau)$ is some lowpass waveform centered at $\tau = 0$. We shall see in the next chapter that the difference between the relative noise phase ϕ_{12}^n and relative signal phase ϕ_{12} (defined in Chapter 2) is an important parameter in determining the arraying gain. We denote this quantity by $\psi_{12} \triangleq \phi_{12}^n - \phi_{12}$.

Note that in deriving (3.19), we have considered the noise generated by the background source only. As mentioned in Chapter 2, however, the additive noise present with the telemetry signal is actually composed of background noise plus that due to receiver electronics. Nevertheless, (3.19) can still be used to describe the cross-correlation, since the noises due to electronics at distinct receivers are independent. Furthermore, it should be noted that (3.19) closely resembles the form of the *auto-*

correlation function for the complex baseband noise observed at a single antenna. Specifically, for noise with a one-sided power spectral density level of N_o W/Hz, the autocorrelation is given by

$$R_{nn}(\tau) = E[n(t)n^*(t-\tau)] = N_o G(\tau) \tag{3.20}$$

Let the *correlation coefficient* between the noise at two antennas be defined as

$$\rho = \frac{|\alpha|}{\sqrt{N_{o_1} N_{o_2}}} \tag{3.21}$$

An upper limit for ρ is found by assuming that the source is in the peak of both antenna patterns, and is very small compared to the fringe period. In this case,

$$\begin{aligned} \alpha &= \frac{\sqrt{A_{e_1} A_{e_2}}}{2} S \\ &= k\sqrt{T_{s_1} T_{s_2}} \end{aligned} \tag{3.22}$$

where T_{s_1} and T_{s_2} are the system temperature increases due to the source at the individual antennas. Combining (3.22) with (3.21) yields

$$\rho = \sqrt{\frac{T_{s_1} T_{s_2}}{T_1 T_2}} \tag{3.23}$$

where T_1 and T_1 are the *total* system temperatures at the two antennas.

3.4 Experimental Data

To illustrate the basic concepts of noise correlation due to a common background, an experiment was conducted as part of this thesis using two of the DSN's antennas at the Goldstone, California complex. Observations of 3C84, which is a broad-band radio source, were made at S-band (2.3 GHz) from a 70-m and 34-m dish antenna. The signals were down-converted to baseband, filtered to a one-sided lowpass bandwidth of 115 kHz, sampled at the Nyquist rate of 230 kHz, and recorded on magnetic

tape. The recorded signals were then processed on a Sun workstation to compute the correlation as a function of time. Figure 3-5 shows the normalized correlation ρ and the measured visibility phase over a period of approximately 8 1/2 minutes. A 0.1 second integration time was used to estimate the correlation for each point. The sharp transition approximately 1 minute from the start indicates the time one of the antennas moved from off the source to pointing at it.

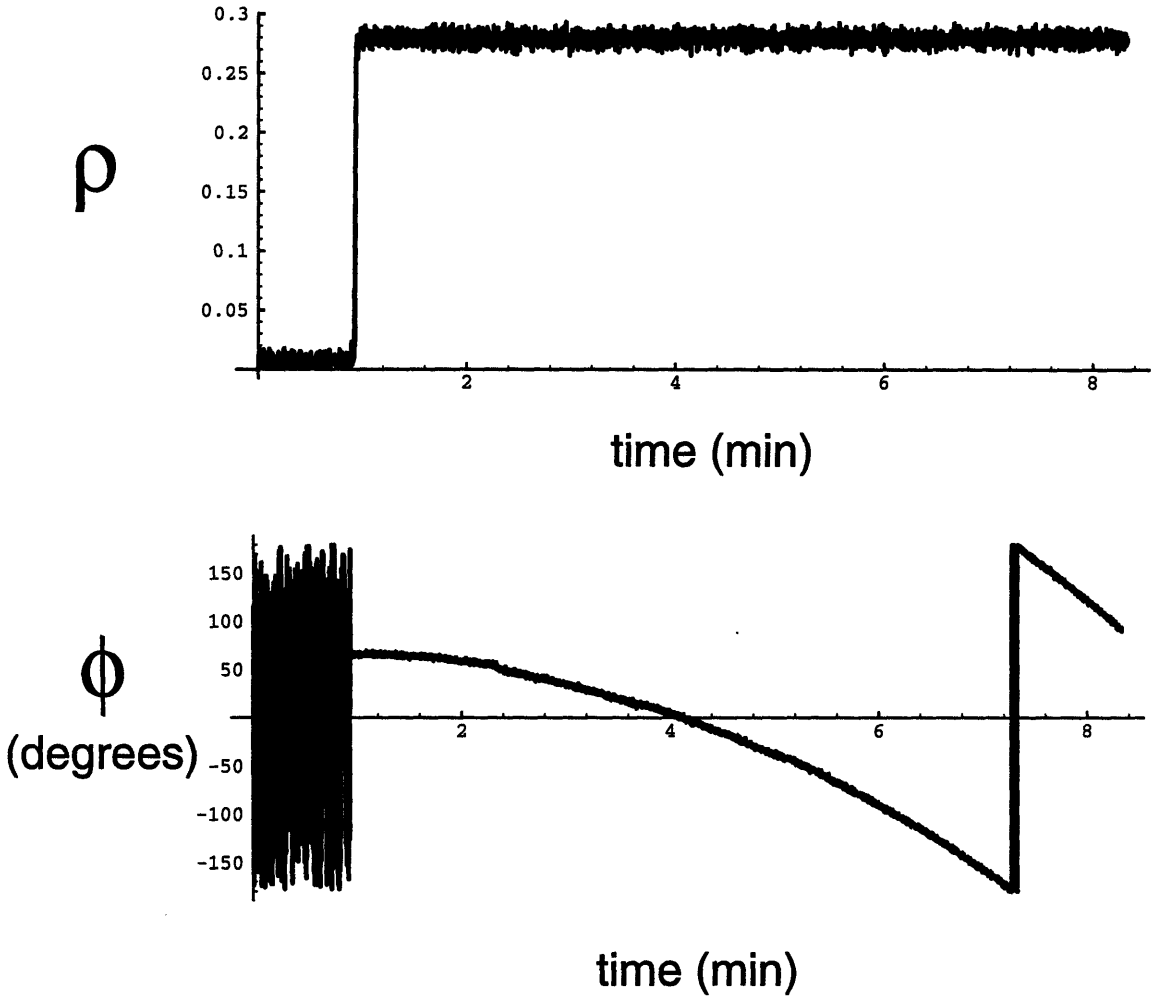

Figure 3-5: Experimental correlation data for 3C84

For the 70-m antenna, the source temperature was measured to be $T_{s_1} = 35.8K$, and the total system temperature (including the source) was measured at $T_1 = 50.3K$. The corresponding temperatures for the 34-m antenna were $T_{s_2} = 7.86K$ and $T_2 = 40.96K$. Note that the contribution of the radio source to the 70-m system temper-

ature is roughly four times greater due to the ratio of the collecting areas. Based on these numbers, the upper bound for the correlation coefficient, using (3.23), is $\rho \leq 0.37$. The mean correlation coefficient measured is approximately 0.26. This difference can be explained by the "resolving" effect. The physical separation between the two antennas is 500 m, from which we conclude the fringe spacing, given by $w = c/(f_o D_p)$, is on the order of 3×10^{-4} radians. The angular size of 3C84 is comparable to this, being approximately 1×10^{-3} radians. Thus, some decrease in the correlation is expected due to averaging over the fringe oscillations.

The above example illustrates how physical parameters such as source size, baseline length, observation frequency, and source and system temperature can be combined to form a rough estimate of what degree of noise correlation can be expected for a given scenario.

Chapter 4

Full Spectrum Combining Performance

This chapter contains a quantitative evaluation of full spectrum combining performance in the presence of correlated noise. In Chapter 2, it was noted that both the ideal arraying gain, G_A, and the arraying degradation, D, are different when correlated noise is present relative to the case of uncorrelated noise. Section 1 evaluates G_A in terms of the noise correlation parameters ρ_{ij} and ψ_{ij} described in the previous chapter. Section 2 then computes the degradation due to imperfect synchronization for full spectrum combining, D_{fsc}. We will see that a major difficulty caused by the noise correlation is the issue of phasing the array. The conventional phase estimation scheme, discussed in [1] and [2], is described, and a modified method to offset the problems caused by noise correlation is proposed. An expression for the arrayed symbol SNR, taking into account phase-alignment and demodulation losses, is then presented, and the degradation is computed. Finally, the analytical results are compared to values obtained by simulation in Section 3.

4.1 Ideal Arraying Gain

Consider an array consisting of L antennas. Recalling the signal format for deep-space telemetry presented in Chapter 2, the complex baseband signal from the i^{th} antenna

can be expressed as

$$\begin{aligned}\tilde{r}_i(t) &= \tilde{s}_i(t) + \tilde{n}_i(t) \\ &= \sqrt{P_{C_i}} e^{j(\omega_b t + \theta_{c_i})} + j\sqrt{P_{D_i}} d(t)\ \mathrm{sqr}(\omega_{sc} t + \theta_{sc}) e^{j(\omega_b t + \theta_{c_i})} + \tilde{n}_i(t) \end{aligned} \quad (4.1)$$

From (2.21), the combined baseband signal for full spectrum combining can be expressed as

$$\begin{aligned}\tilde{r}_{comb}(t) &= \tilde{s}_{comb}(t) + \tilde{n}_{comb}(t) \\ &= \sum_{i=1}^{L} \beta_i \left(\tilde{s}_i(t) + \tilde{n}_i(t)\right) e^{j\phi_{1i}} \\ &= e^{j(\omega_b t + \theta_1)} \sum_{i=1}^{L} \beta_i \left(\sqrt{P_{C_i}} + j\sqrt{P_{D_i}}\, d(t)\ \mathrm{sqr}(\omega_{sc} t + \theta_{sc})\right) \\ &\quad + \sum_{i=1}^{L} \beta_i \tilde{n}_i(t)\, e^{j\phi_{1i}} \end{aligned} \quad (4.2)$$

where we have assumed the i^{th} signal has been phase-rotated by an amount ϕ_{1i} to compensate for the difference in carrier phase between the 1^{st} and i^{th} antenna. If all the noise processes $\tilde{n}_i(t)$ are uncorrelated, the SNR of the combined signal is maximized if the weights β_i are chosen to satisfy the condition

$$\beta_i = \sqrt{\frac{P_{T_i}}{P_{T_1}} \frac{N_{o1}}{N_{oi}}} \quad (4.3)$$

for $i = 1 \ldots L$. Note, however, that this is *not* the optimal choice of weights in the case of correlated noise waveforms. Furthermore, the optimal choice of phases used to array the signals is not necessarily the relative signal phases, ϕ_{1i}. Using the phases ϕ_{1i} will certainly maximize the arrayed signal power, but not necessarily the *ratio* of signal to noise power, which is the relevant criteria for optimization. The problem of optimal combining weights and phases for signals with correlated noise has been analyzed in [7], where the results are applied to an array of antenna feed elements. However, computation of these weights requires knowledge of the pairwise correlations between the noises, $\alpha_{ij} e^{j\phi^n_{ij}}$. A scheme can be devised to estimate the required parameters in

real time and modify the weights accordingly, but would significantly complicate the problem. Our goal, instead, is to determine the performance impact of the correlated noise assuming the traditional combining scheme is used.

The total combined signal power, P_T, is given by

$$P_T \triangleq E[\tilde{s}_{comb}(t)]\, E[\tilde{s}^*_{comb}(t)] \tag{4.4}$$

If the weighting factors are chosen according to 4.3, the combined signal power becomes

$$P_T = P_{T_1}\left(\sum_{i=1}^{L}\gamma_i^2 + \sum_{i=1}^{L}\sum_{\substack{j=1\\ i\neq j}}^{L}\gamma_i\gamma_j\right) \tag{4.5}$$

where $\gamma_i \triangleq \frac{P_{T_i}}{P_{T_1}}\frac{N_{o_1}}{N_{o_i}}$.

The one-sided power spectral density of the real and imaginary parts of the combined noise is given by

$$N_o \triangleq \frac{1}{2B}E[\tilde{n}_{comb}(t)\ \tilde{n}^*_{comb}(t)] \tag{4.6}$$

where B is the one-sided bandwidth of the noise waveforms. Note that the factor of two in the denominator of (4.6) results from the fact that the real and imaginary parts of the noise each has half the power of the complex noise. From the definitions of power spectral density and cross power spectral density, it follows that

$$E[\tilde{n}_i(t)\tilde{n}^*_i(t)] = 2N_{o_i}B \tag{4.7}$$

$$E[\tilde{n}_i(t)\tilde{n}^*_j(t)] = 2\alpha_{ij}e^{\phi^n_{ij}}B \tag{4.8}$$

Equations (4.6), (4.7), and (4.8) can be combined to find the power spectral density of the combined noise, yielding

$$N_o = N_{o_1}\left(\sum_{i=1}^{L}\gamma_i + \sum_{i=1}^{L}\sum_{\substack{j=1\\ i\neq j}}^{L}\sqrt{\gamma_i\gamma_j}\rho_{ij}e^{j(\phi^n_{ij}-\phi_{ij})}\right) \tag{4.9}$$

The P_T/N_o of the combined signal is thus given by

$$\frac{P_T}{N_o} = \frac{P_{T_1}}{N_{o_1}} \frac{\left(\sum_{i=1}^{L} \gamma_i\right)^2}{\sum_{i=1}^{L} \gamma_i + \sum_{i=1}^{L} \sum_{\substack{j=1 \\ i \neq j}}^{L} \sqrt{\gamma_i \gamma_j}\, \rho_{ij}\, e^{j\psi_{ij}}} \tag{4.10}$$

where $\psi_{ij} = \phi_{ij}^n - \phi_{ij}$, as defined in Chapter 3. The parameters ρ_{ij} and ψ_{ij} describe the relevant statistics for the noise correlations between the various antenna pairs, and determine the correlated noise impact on the ideal arraying gain.

The combined signal is finally processed by a single carrier, subcarrier, and symbol loop. Assuming perfect references at each of these three stages, the symbol SNR of the arrayed signal becomes

$$\begin{aligned} SNR_{ideal} &= \frac{2P_{D_1}}{N_{o_1} R_{sym}} \frac{(\sum_{i=1}^{L} \gamma_i)^2}{\sum_{i=1}^{L} \gamma_i + \sum_{i=1}^{L} \sum_{\substack{j=1 \\ i \neq j}}^{L} (\gamma_i \gamma_j)^{1/2} \rho_{ij}\, e^{j\psi_{ij}}} \\ &= \frac{2P_{D_1}}{N_{o_1} R_{sym}} G_A \end{aligned} \tag{4.11}$$

where G_A is the ideal arraying gain due to combining the signals. Note that setting all the noise correlation coefficients ρ_{ij} to zero results in $G_A = \sum_{i=1}^{L} \gamma_i$, which is the ideal arraying gain in the case of uncorrelated noises, as discussed in [1].

Further note that the ideal arraying gain in the presence of correlated noise can be higher *or* lower than the uncorrelated noise case, depending on the phases ψ_{ij}. The intuitive reason for this can be understood by considering an array of two equal antennas (i.e., $\gamma_1 = \gamma_2 = 1$.) Figure 4-1 shows values for G_A for two equal antennas as a function of ρ and ψ. For $\rho = 0$, the ideal arraying gain is a constant 3 dB, as expected. Now suppose the noises have some nonzero correlation coefficient ρ, and some correlation phase ϕ^n. If $\psi = 0°$, then the phase difference of the spacecraft signal as observed by antennas 1 and 2, ϕ, is equal to the noise correlation phase ϕ^n. Thus, phase-aligning the two signals *also* phase-aligns the correlated component of the noise. The noise from the background source adds maximally in phase, and the combined noise power increases. Thus, the combined SNR decreases, and hence the arraying gain falls below 3 dB. By contrast, if $\psi = 180°$, phase-aligning the signal

results in combining the correlated component of the noise 180° out of phase. Thus, the noise combines destructively in this case, and the arraying gain is now *greater* than 3 dB. For intermediate values of ψ, the arraying gain varies continuously from its minimum value at $\psi = 0°$ to its maximum at $\psi = 180°$.

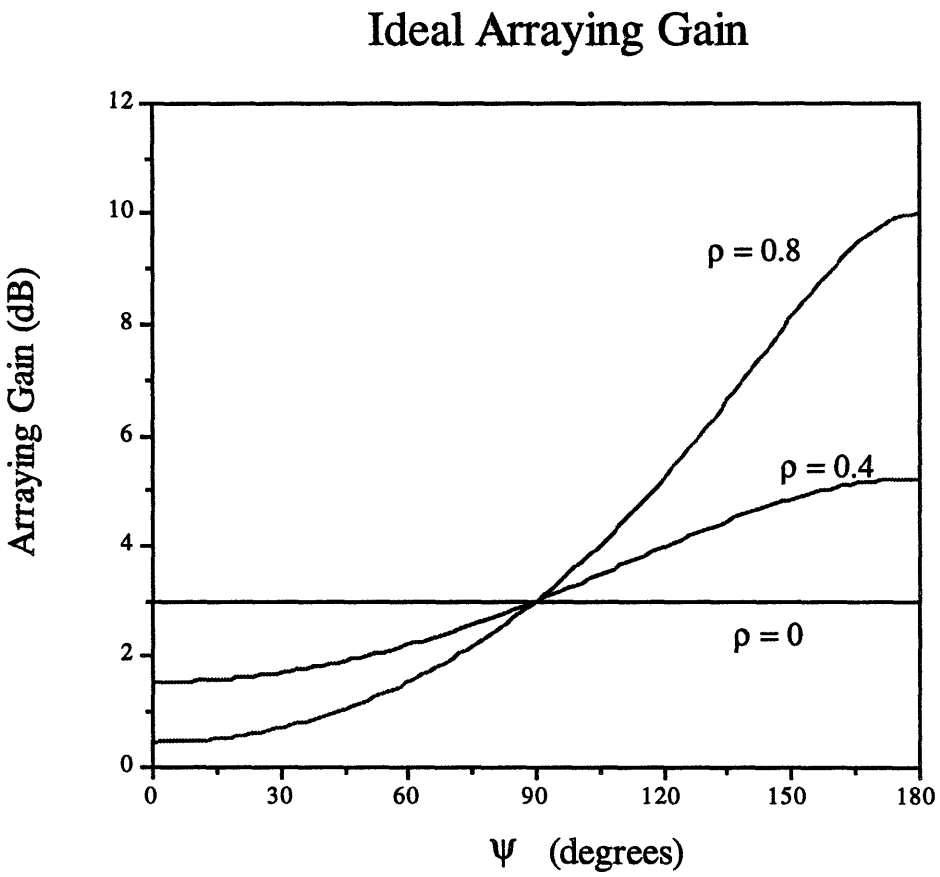

Figure 4-1: Ideal arraying gain G_A for various ρ, ψ

4.2 Symbol SNR Degradation

In practice, perfect phase alignment and ideal carrier, subcarrier, and symbol references are not available. Some degradation in the arrayed symbol SNR is therefore incurred due to synchronization errors. To quantify the degradation, we first find the set of density functions for the phase alignment errors $\Delta\phi_{1i} \triangleq \hat{\phi}_{1i} - \phi_{1i}$, $i = 2 \ldots L$. This set of functions is then used to compute the P_T/N_o of the arrayed signal. Adding in losses due to carrier, subcarrier, and symbol tracking, the symbol SNR at the

matched filter output can be computed. Finally, comparing the actual symbol SNR to the ideal symbol SNR given by (4.11) yields the degradation for full spectrum combining.

4.2.1 Antenna Phasing

A set of phase estimates $\hat{\phi}_{1i}$ for $i = 2 \ldots L$ are needed to align signals $2 \ldots L$ with signal 1. In the description of FSC given in [2], the phase difference between $\tilde{s}_i(t)$ and $\tilde{s}_1(t)$ is estimated by filtering the two signals to some lowpass bandwidth B_{lp} Hertz, multiplying them, and averaging their product over T_{corr} seconds. The phase of this complex quantity is then computed by taking the inverse tangent of the ratio of the imaginary to real parts. A block diagram of this scheme is shown in Figure 4-2.

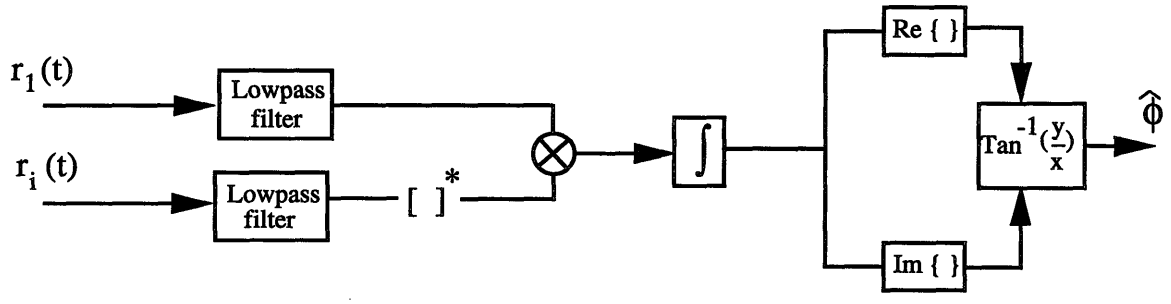

Figure 4-2: Conventional phase estimator

The complex product of the baseband signals after averaging, Z, is given by

$$\begin{aligned} Z &= \frac{1}{T_{corr}} \int (\tilde{s}_{lp_1}(t) + \tilde{n}_{lp_1}(t))(\tilde{s}^*_{lp_i}(t) + \tilde{n}^*_{lp_i}(t)) \\ &= (\sqrt{P_{C_1} P_{C_i}} + \sqrt{P_{D_1} P_{D_i}} H) e^{j\phi_{1i}} + \frac{1}{T_{corr}} \int \left(\tilde{n}_{s,n}(t) + \tilde{n}_{lp_1}(t) \tilde{n}^*_{lp_i}(t) \right) \, dt \end{aligned} \tag{4.12}$$

where H is given by

$$H = \left(\frac{4}{\pi}\right)^2 \sum_{\substack{i=1 \\ i \text{ odd}}}^{M} \frac{1}{2i^2} \tag{4.13}$$

and M is the highest harmonic of the subcarrier passed by the lowpass filter. The term $\tilde{n}_{s,n}(t)$ is composed of signal-noise terms in the product and has zero mean.

Note, however, that the noise-noise term, $\tilde{n}_{lp_1}(t)\tilde{n}^*_{lp_i}(t)$, does not necessarily have zero mean, due to a possible correlation that exists between the two noise waveforms. The expected value of this noise product can easily be computed from the cross power spectral density of $\tilde{n}_1(t)$ and $\tilde{n}_i(t)$; thus,

$$E[Z] = (\sqrt{P_{C_1}P_{C_i}} + \sqrt{P_{D_1}P_{D_i}}H)e^{j\phi_{1i}} + 2\rho_{1i}\sqrt{N_{o_1}N_{o_i}}B_{lp}e^{j\phi^n_{1i}} \tag{4.14}$$

Since ϕ^n_{1i} is not necessarily equal to ϕ_{1i}, the noise product introduces a "bias" to the estimate of the relative signal phase. This situation can be represented pictorially in Figure 4-3. The complex quantity $E[z]$ can be thought of as a vector sum of a signal-

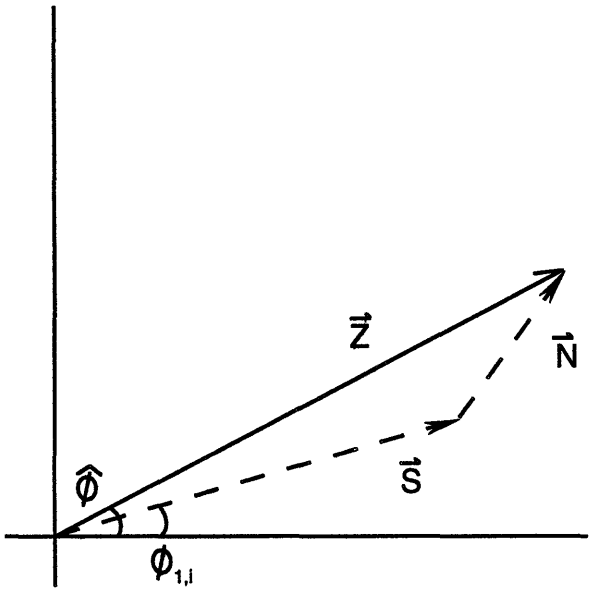

Figure 4-3: Complex correlation vector

to-signal correlation, $\vec{S}$, and a noise-to-noise correlation, $\vec{N}$. Note how the presence of the noise vector biases the measurement of the phase of the complex correlation. The relative magnitude of these vectors is given by

$$\frac{|\vec{S}|}{|\vec{N}|} = \frac{1}{2\rho_{1i}\,B_{lp}}\left(\left(\frac{P_{C_1}}{N_{o_1}}\frac{P_{C_i}}{N_{o_i}}\right)^{1/2} + H\left(\frac{P_{D_1}}{N_{o_1}}\frac{P_{D_i}}{N_{o_i}}\right)^{1/2}\right) \tag{4.15}$$

For typical parameters, even relatively modest levels of noise correlation can lead to a substantial biasing effect in estimating the relative signal phase. For example, consider

correlating two signals each having a P_T/N_o of 20 dB-Hz with a 1 kHz correlation bandwidth. Even if all subcarrier harmonics are included in the correlation, making $H = 1$, a correlation coefficient as low as $\rho = 0.1$ makes the ratio in (4.15) equal to 0.5. The phase estimates are then influenced more by the relative *noise* phases ϕ_{1i}^n than the desired quantities ϕ_{1i}, leading to a high amount of degradation in combining the signals. A practical implementation of full spectrum combining therefore requires a modified phase estimation algorithm if correlation levels encountered will generate significant biases.

The method of phase estimation shown in Figure 4-4 can be used for this purpose. Here, each signal is filtered to some bandpass bandwidth B_{bp}, and an additional complex correlation is performed between the resulting waveforms. The center frequency of this filter is chosen so as to *not* capture any energy from the telemetry; this can be

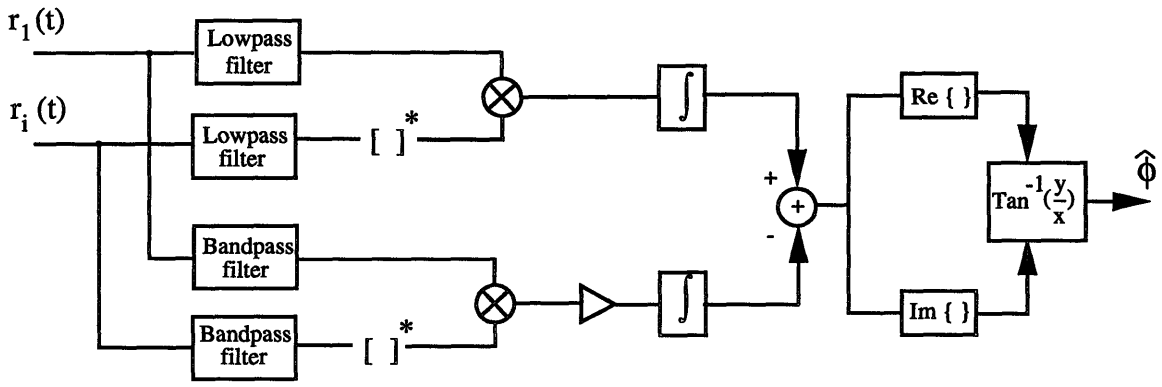

Figure 4-4: Modified phase estimator

accomplished by locating the filter at an even multiple of the subcarrier frequency, for example. After scaling the noise-only correlation by the ratio of the lowpass to bandpass bandwidths, this quantity provides an estimate of the contribution of the noise to the total correlation. The bandpass correlation can then be subtracted from the lowpass correlation to compensate for the mean correlation vector $|\vec{N}|$. The compensated correlation can thus be expressed as

$$\begin{aligned} Z &= (\sqrt{P_{C_1}P_{C_i}} + \sqrt{P_{D_1}P_{D_i}}H)e^{j\phi_{1i}} + \frac{1}{T_{corr}}\int \left(\tilde{n}_{s,n}(t) + \tilde{n}_{lp_1}(t)\tilde{n}^*_{lp_i}(t)\right)\, dt \\ &\quad - \frac{B_{lp}}{B_{bp}}\frac{1}{T_{corr}}\int \tilde{n}_{bp_1}(t)\tilde{n}^*_{bp_i}(t)\, dt \end{aligned}$$

$$= (\sqrt{P_{c1}P_{ci}} + \sqrt{P_{d1}P_{di}}H)e^{j\phi_{1i}} + \tilde{N} \tag{4.16}$$

where the the noise term $\tilde{N}$ now has zero mean. The phase estimate is then found by taking the inverse tangent of the ratio of the imaginary to real part of (4.16), i.e.,

$$\hat{\phi}_{1i} = \tan^{-1}\left[\frac{(\sqrt{P_{C_1}P_{C_i}} + \sqrt{P_{D_1}P_{D_i}}H)\ \sin\phi_{1i} + N_Q}{(\sqrt{P_{C_1}P_{C_i}} + \sqrt{P_{D_1}P_{D_i}}H)\ \cos\phi_{1i} + N_I}\right] \tag{4.17}$$

where N_I and N_Q are the real and imaginary parts of $\tilde{N}$, respectively. Note that although N_I and N_Q have zero mean, their joint statistics are *still* influenced by the correlation between $\tilde{n}_1(t)$ and $\tilde{n}_i(t)$. These statistics are analyzed in Appendix A, and the density function for the phase estimation error $\Delta\phi_{1i} \triangleq \hat{\phi}_{1i} - \phi_{1i}$ is derived.

In [2], a quantity known as the *correlator SNR* is introduced, defined as

$$SNR_{corr} = \frac{E[Z]E^*[Z]}{E[ZZ^*] - E[Z]E^*[Z]} \tag{4.18}$$

The correlator SNR is a measure of the spread of the phase error density $p_\phi(\Delta\phi_{1i})$, and is inversely related to the variance of the phase error. In [1], where FSC is analyzed for independent noises, it is shown that the phase error density can be expressed solely in terms of the correlator SNR. For the correlated noise case, the density is given in Appendix A in terms of the correlator SNR and the correlation parameters ρ_{1i} and ψ_{1i}.

Figures 4-5 - 4-7 show the density function $p_\phi(\Delta\phi)$ for various values of ρ and ψ. The signal parameters chosen for these curves are $(P_T/N_o)_1 = (P_T/N_o)_2 = 25$ dB-Hz, $\Delta = 90$ deg, with seven subcarrier harmonics included in the correlation. The correlator parameters are $B_{lp} = B_{bp} = 15$ kHz, and $T_{corr} = 3$ seconds. Note that even for a noise correlation as high as 0.4, the density function looks remarkably like that of the uncorrelated noise case. Simulations were performed for the same parameters, and densities collected for the measured phase estimates. These results are shown with the analytical curves in Figure 4-8.

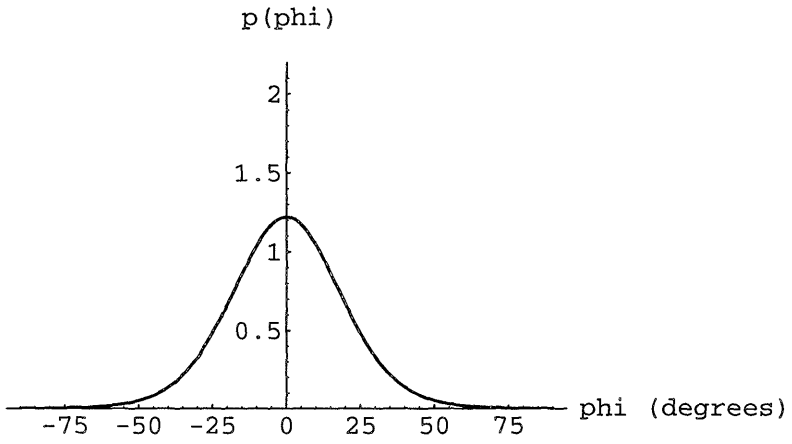

$$\rho = 0$$

Figure 4-5: Phase estimate density

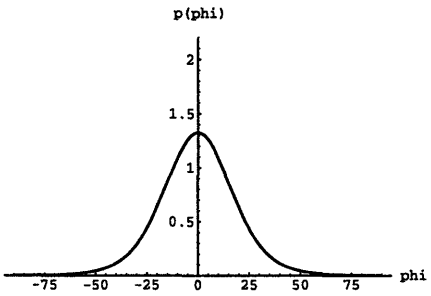

$\rho = 0.4, \quad \psi = 0$ degrees

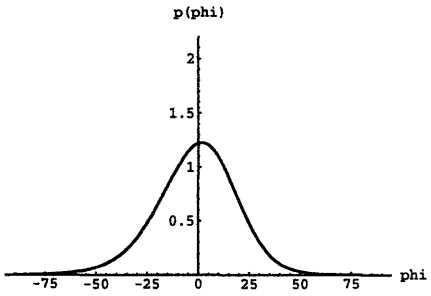

$\rho = 0.4, \quad \psi = 45$ degrees

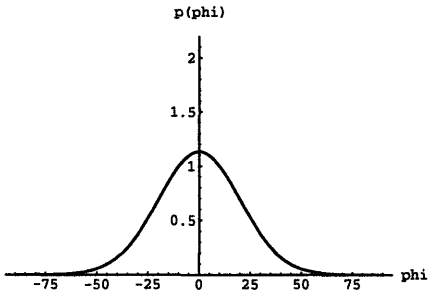

$\rho = 0.4, \quad \psi = 90$ degrees

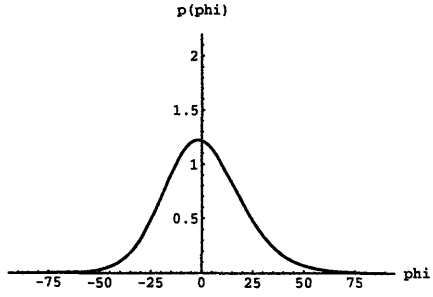

$\rho = 0.4, \quad \psi = 135$ degrees

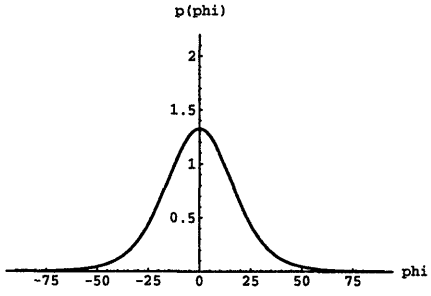

$\rho = 0.4, \quad \psi = 180$ degrees

Figure 4-6: Phase estimate densities

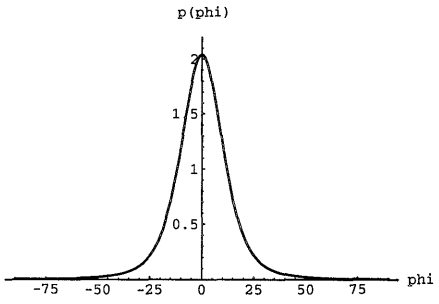

$\rho = 0.8, \quad \psi = 0$ degrees

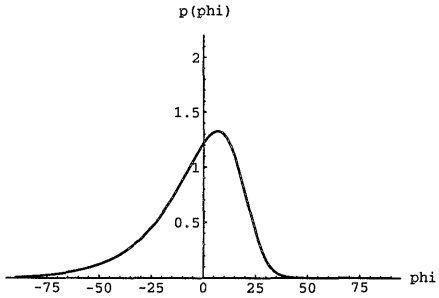

$\rho = 0.8, \quad \psi = 45$ degrees

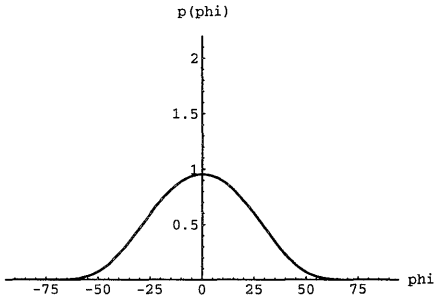

$\rho = 0.8, \quad \psi = 90$ degrees

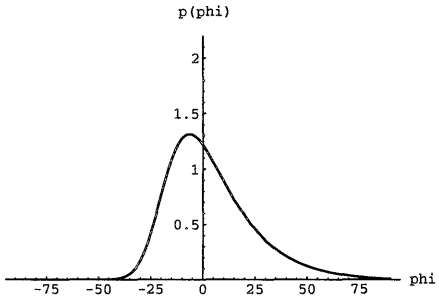

$\rho = 0.8, \quad \psi = 135$ degrees

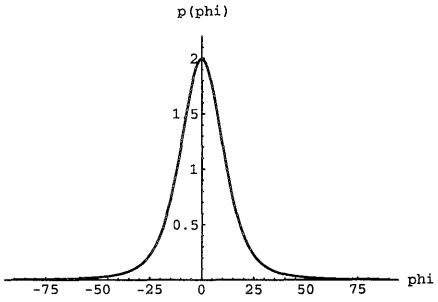

$\rho = 0.8, \quad \psi = 180$ degrees

Figure 4-7: Phase estimate densities

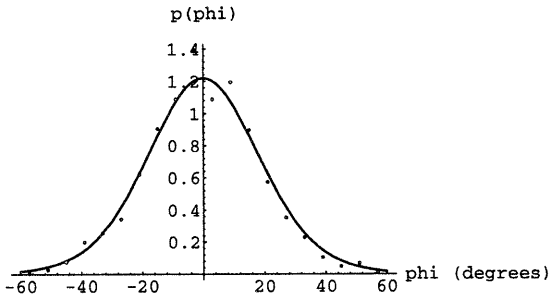

$\rho = 0.0$

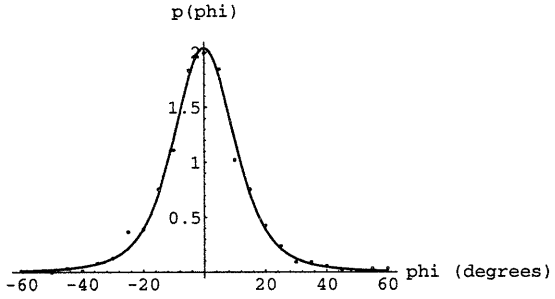

$\rho = 0.8,\ \psi = 0$ degrees

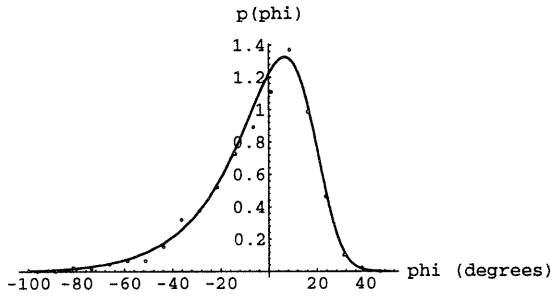

$\rho = 0.8,\ \psi = 45$ degrees

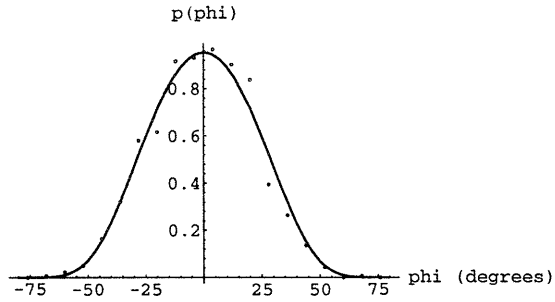

$\rho = 0.8,\ \psi = 90$ degrees

Figure 4-8: Phase estimate densities with simulation points

4.2.2 Arrayed Symbol SNR and Symbol SNR Degradation

Using the set of estimated phases to align the signals, the combined signal becomes

$$\tilde{r}_{comb}(t) = \tilde{s}_{comb}(t) + \tilde{n}_{comb}(t) \tag{4.19}$$

$$= \sum_{i=1}^{L} \beta_i \, e^{j\hat{\phi}_{1i}} \tilde{s}_i(t) + \sum_{i=1}^{L} \beta_i \, e^{j\hat{\phi}_{1i}} \tilde{n}_i(t) \tag{4.20}$$

$$= \sum_{i=1}^{L} \beta_i \, (\sqrt{P_{C_i}} + j\sqrt{P_{D_i}} \, \mathrm{sqr}(\omega_{sc}t + \theta_{sc}))e^{j(\omega_i t + \theta_1 + \Delta\phi_{1i})}$$
$$+ \sum_{i=1}^{L} \beta_i \, e^{j\hat{\phi}_{1i}} \tilde{n}_i(t) \tag{4.21}$$

The combined signal power conditioned on the set of phase errors $\Delta\phi_{1i}$ is thus given by

$$P_T' = E[\tilde{s}_{comb}(t)]E[\tilde{s}^*_{comb}(t)] \tag{4.22}$$
$$= P_{T_1}\left(\sum_{i=1}^{L}\gamma_i^2 + \sum_{i=1}^{L}\sum_{\substack{j=1 \\ i\neq j}}^{L}\gamma_i\gamma_j e^{j(\Delta\phi_{1i}-\Delta\phi_{1j})}\right) \tag{4.23}$$

Similarly, the conditional noise power spectral density is given by

$$N_o' = \frac{1}{2B}E[\tilde{n}_{comb}(t)\tilde{n}^*_{comb}(t)] \tag{4.24}$$
$$= N_{o_1}\left(\sum_{i=1}^{L}\gamma_i + \sum_{i=1}^{L}\sum_{\substack{j=1 \\ i\neq j}}^{L}(\gamma_i\gamma_j)^{1/2}\rho_{ij}\, e^{j\psi_{ij}}\, e^{j(\Delta\phi_{1i}-\Delta\phi_{1j})}\right) \tag{4.25}$$

Taking the ratio of (4.23) to (4.25) yields the conditonal P_T/N_o of the combined signal, i.e.,

$$(\frac{P_T}{N_o})' = \frac{P_{T1}}{N_{o1}} \frac{\sum_{i=1}^{L}\gamma_i^2 + \sum_{i=1}^{L}\sum_{\substack{j=1 \\ i\neq j}}^{L}\gamma_i\gamma_j e^{j(\Delta\phi_{1i}-\Delta\phi_{1j})}}{\sum_{i=1}^{L}\gamma_i + \sum_{i=1}^{L}\sum_{\substack{j=1 \\ i\neq j}}^{L}(\gamma_i\gamma_j)^{1/2}\,\rho_{ij}\, e^{j\psi_{ij}}\, e^{j(\Delta\phi_{1i}-\Delta\phi_{1j})}} \tag{4.26}$$

After carrier and subcarrier demodulation and matched filtering, the conditional symbol SNR of the arrayed signal is given by

$$SNR' = \frac{2P_{T1}}{N_{o1}R_{sym}} \frac{\sum_{i=1}^{L}\gamma_i^2 + \sum_{i=1}^{L}\sum_{\substack{j=1 \\ i\neq j}}^{L}\gamma_i\gamma_j e^{j(\Delta\phi_{1i}-\Delta\phi_{1j})}}{\sum_{i=1}^{L}\gamma_i + \sum_{i=1}^{L}\sum_{\substack{j=1 \\ i\neq j}}^{L}(\gamma_i\gamma_j)^{1/2}\rho_{ij}e^{j\psi_{ij}}\, e^{j(\Delta\phi_{1i}-\Delta\phi_{1j})}} \; C_c^2 C_{sc}^2 C_{sy}^2 \tag{4.27}$$

where C_c, C_{sc}, and C_{sy} are the carrier, subcarrier, and symbol reduction functions, respectively. The unconditional symbol SNR is obtained by integrating (4.27) over the density functions for $\hat{\phi}_{21} \ldots \hat{\phi}_{L1}$ and the loop errors ϕ_c, ϕ_{sc}, and ϕ_{sy}. In order

to simplify this computation, the loop errors and phase estimates are generally assumed to be independent. Taking expectation with respect to each of these quantities separately yields an expression for the unconditional symbol SNR, namely

$$SNR = \frac{2P_{T1}}{N_{o1}R_{sym}} \overline{C_c^2}\,\overline{C_{sc}^2}\,\overline{C_{sy}^2} \times \int_{-\pi}^{\pi}\cdots\int_{-\pi}^{\pi}\left[\frac{\sum_{i=1}^{L}\gamma_i^2 + \sum_{i=1}^{L}\sum_{\substack{j=1\\ i\neq j}}^{L}\gamma_i\gamma_j e^{j(\Delta\phi_{1i}-\Delta\phi_{1j})}}{\sum_{i=1}^{L}\gamma_i + \sum_{i=1}^{L}\sum_{\substack{j=1\\ i\neq j}}^{L}(\gamma_i\gamma_j)^{1/2}\rho_{ij}\, e^{j\psi_{ij}}\, e^{j(\Delta\phi_{1i}-\Delta\phi_{1j})}}\right. \left. p(\Delta\phi_{1i})\cdots p(\Delta\phi_{1L})\right] d\Delta\phi_{12}\cdots d\Delta\phi_{1L} \tag{4.28}$$

where $\overline{C_c^2}$, $\overline{C_{sc}^2}$, and $\overline{C_{sy}^2}$ are given by (2.13) - (2.15) in terms of the respective loop SNRs, and the density functions $p_\phi(\Delta\phi_{1i})$ are as given in Appendix A. Note that the *arrayed* P_T/N_o is used to calculate the three loop SNRs, each of the three loops is tracking the combined signal. Taking the ratio of (4.28) to the ideal SNR, (4.11), yields the degradation for full spectrum combining:

$$D_{fsc} = \overline{C_c^2}\,\overline{C_{sc}^2}\,\overline{C_{sy}^2} \int_{-\pi}^{\pi}\cdots\int_{-\pi}^{\pi}\left[\frac{\sum_{i=1}^{L}\gamma_i^2 + \sum_{i=1}^{L}\sum_{\substack{j=1\\ i\neq j}}^{L}\gamma_i\gamma_j e^{j(\Delta\phi_{1i}-\Delta\phi_{1j})}}{\sum_{i=1}^{L}\gamma_i + \sum_{i=1}^{L}\sum_{\substack{j=1\\ i\neq j}}^{L}(\gamma_i\gamma_j)^{1/2}\rho_{ij}\, e^{j\psi_{ij}}\, e^{j(\Delta\phi_{1i}-\Delta\phi_{1j})}}\right. \left. p(\Delta\phi_{1i})\cdots p(\Delta\phi_{1L})\right] d\Delta\phi_{12}\cdots d\Delta\phi_{1L}\; G_A^{-1} \tag{4.29}$$

Note that D_{fsc} is equal to one in the upper limit, where $\Delta\phi_{1i} = 0$ for $i = 2\ldots L$ and $\overline{C_c^2} = \overline{C_{sc}^2} = \overline{C_{sy}^2} = 1$.

4.3 Simulation Results

A simple two-antenna array was simulated under conditions of correlated noise to verify the analysis given above. The symbol SNR of the combined data was measured using an SNR estimator known as the split-symbol moments estimator, and divided by the ideal symbol SNR to obtain measured degradations. The signal parameters used were $P_{T_1}/N_{o_1} = P_{T_2}/N_{o_2} = 25$ dB-Hz, $R_{sym} = 200$ sps, and $\Delta = 90$ degrees. The carrier, subcarrier, and symbol loops were operated with bandwidths of 3.5 Hz,

0.75 Hz, and 0.15 Hz, respectively, with a symbol window of 1/2. The correlation coefficient between the noises, ρ, and the relative noise phase, ψ were varied over a range of values.

Figure 4-9 shows simulation values along with curves describing analytical results for a "high" correlator SNR. The correlation bandwidths and integration time were chosen so that degradation resulting from imperfect phasing are negligible compared to the carrier, subcarrier, and symbol losses. The curves show that more degradation is incurred with increasing noise correlation for $\psi = 0°$, and that degradation decreases as ρ increases for $\psi = 180°$[1] This can be explained by noting the effect of varying ρ and ψ on the arraying gain. For $\psi = 0°$, increasing ρ causes a decrease in arrayed symbol SNR, as explained in Section 3.1. The loop SNR of the three loops therefore decreases, resulting in more carrier, subcarrier, and symbol loss. By contrast, when $\psi = 180°$, increasing ρ increases the combined P_T/N_o, and raises the three loop SNRs. This results in *less* degradation in demodulating the signal. Since the correlator SNR is high in this example, the demodulation losses are the dominant source of degradation, and the trend shown in Figure 4-9 is thus explained.

Figure 4-10 shows the same results performed for a relatively "low" correlator SNR. Here, the degradation curve for $\psi = 180°$ actually lies *below* the curve for $\psi = 0$ degrees. This result, although seemingly counter-intuitive, can nevertheless be explained qualitatively. Note from (4.27) that the phase error terms $\Delta\phi_{1i}$ appear in both the numerator *and* the denominator of the SNR expression; the phase errors affect both the arrayed signal power and the arrayed noise power. This is in contrast to the uncorrelated noise case, where only the numerator depends on the phase errors $\Delta\phi_{i1}$; since the noises are uncorrelated, the choice of phases used in combining them does not affect their arrayed power. The phase errors $\Delta\phi_{1i}$ always decrease the arrayed signal power, but can decrease *or* increase the arrayed noise power, depending on the phase parameter ψ. For $\psi = 180°$, the noise power is increased by errors in estimating ϕ_{1i}, since phasing the array perfectly results in maximum noise cancella-

[1]The phrase "decreasing degradation" is used loosely to mean decreased synchronization losses; in actuality, numerically lower degradation implies *greater* losses incurred.

tion. Therefore, estimating the phase imperfectly results in a twofold penalty: the combined signal power is lessened, and the combined noise power increases. This results in increased degradation due to phase alignment. On the other hand, when $\psi = 0°$, phase misalignment *decreases* the arrayed noise power. Since $\phi_{1i} = \phi_{1i}^n$ in this case, aligning the signals imperfectly also lessens the constructive addition of the noise. The reduced noise power due to phasing errors therefore have a mitigating effect on the degradation incurred.

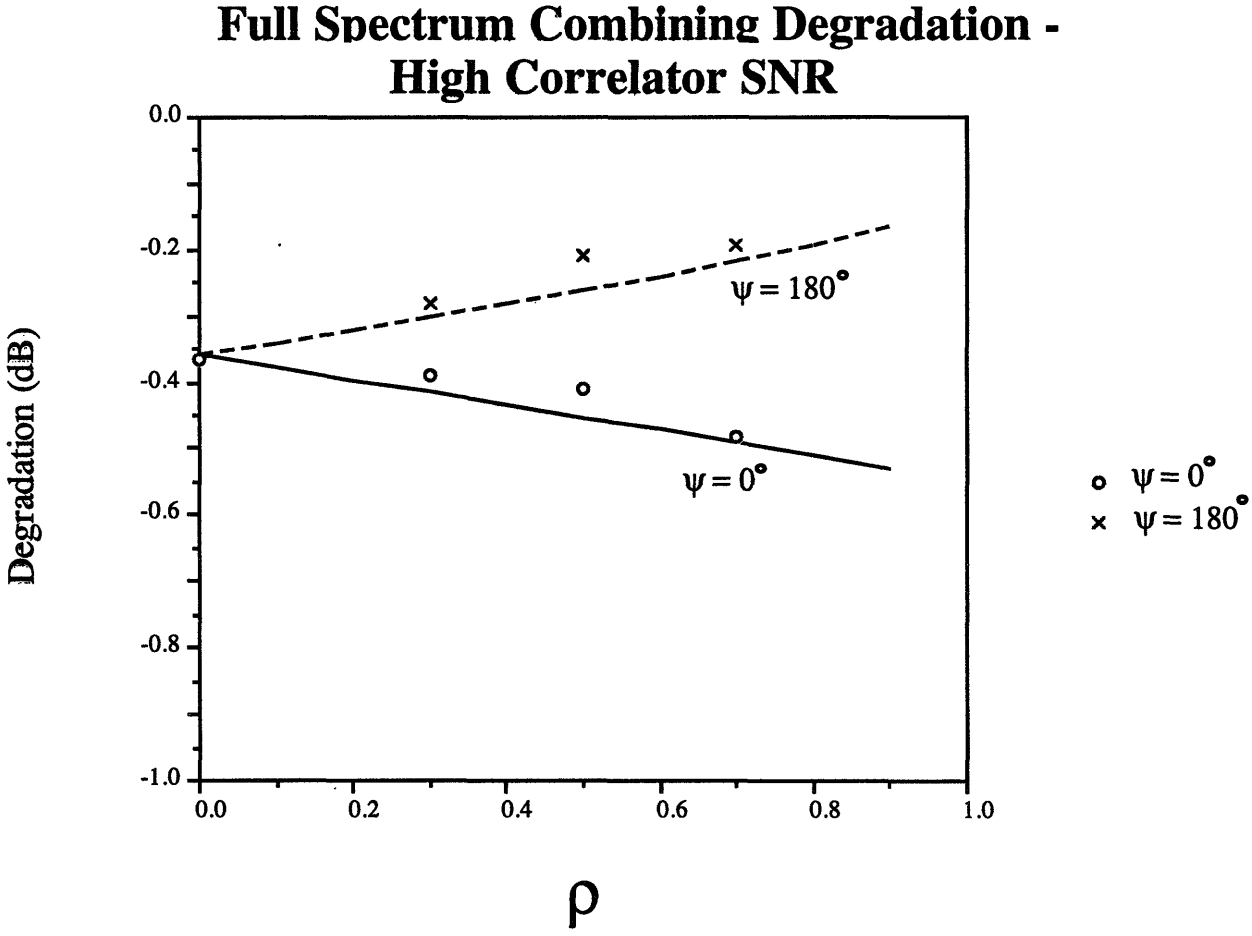

Figure 4-9: FSC degradation - theory and simulation

It should be noted that the fact that the $\psi = 180°$ case has more degradation than the $\psi = 0°$ case in this example does *not* mean that the overall performance of the array is worse for $\psi = 180°$. Recall that degradation is defined as the deviation from the ideal arraying gain, G_A. In the above example, although the degradation for $\psi = 180°$ is slightly higher, the ideal gain is substantially higher than it is for

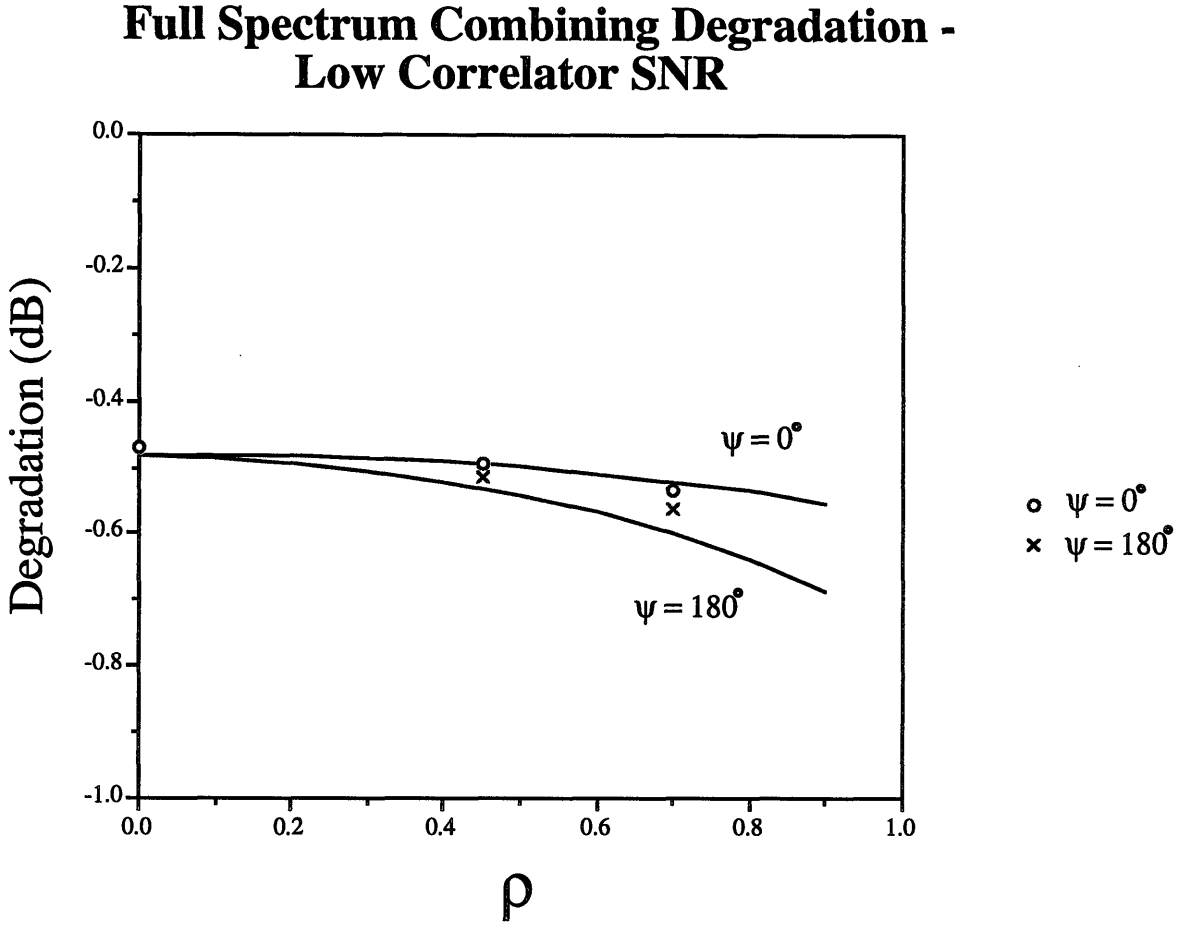

Figure 4-10: FSC degradation - theory and simulation

$\psi = 0°$. Thus, to determine the absolute performance for the array in terms of total combined SNR, both the ideal gain and the degradation must be accounted for.

Chapter 5

Complex Symbol Combining Performance

Here, we analyze the performance of complex symbol combining in a manner that parallels that of the previous chapter. Recall that the expression for SNR_{ideal} is the same for CSC as it is for FSC, as discussed in Chapter 2. Thus, the derivation of the ideal arraying gain for complex symbol combining is omitted here, and the phase-alignment algorithm used for CSC is analyzed in Section 1. Section 2 then computes the arrayed symbol SNR and the symbol SNR degradation. Finally, simulation results are presented and compared to analytical results in Section 3.

It was briefly pointed out in Chapter Two that the subcarrier and symbol tracking performance for CSC is different from that of the conventional receiver, since carrier demodulation is postponed to the end. Since subcarrier and symbol tracking are performed in the absence of carrier lock, the loop SNRs of these loops are different than in the case where coherent carrier demodulation precedes subcarrier and symbol tracking. Two types of subcarrier and symbol loops that may be used in complex symbol combining are discussed in [2]: the conventional, or "I" loop, which uses only one of the two signals in the complex pair to track, and the "IQ" loop, which uses both real and imaginary channels. We will assume the IQ loops are used, since they have higher loop SNRs. Following matched filtering, the complex symbols from each receiver are transmitted to a central location for combining. As in the case of

full-spectrum combining, correlations are performed to phase-align the carriers, after which the signals are weighted and summed coherently. A baseband Costas loop is finally used to demodulate the carrier.

5.1 Antenna phasing

The complex symbol stream from the i^{th} antenna is given by

$$\tilde{Y}_i(k) = \sqrt{P_{d_i}} C_{sc_i} C_{sy_i}\, d(k)\, e^{j(\omega_b T_s k + \theta_i)} + \tilde{N}_i(k) \tag{5.1}$$

where C_{sc_i} and C_{sy_i} are the subcarrier and symbol reduction functions for the i^{th} receiver, T_s is the symbol time, and $N_i(k)$ is the noise output from the i^{th} matched filter. Taking the complex product between the 1^{st} and i^{th} streams yields

$$Z = \tilde{Y}_1(k)\tilde{Y}_i^*(k) = \sqrt{P_{D_1} P_{D_i}} C_{sc_1} C_{sc_i} C_{sy_1} C_{sy_i} + \tilde{N}_{s,n}(k) + \tilde{N}_1(k)\tilde{N}_i^*(k) \tag{5.2}$$

where the signal-noise term $\tilde{N}_{s,n}(k)$ has zero mean. Once again, the complex noise product $\tilde{N}_1(k)\tilde{N}_i^*(k)$ has nonzero mean if the correlation coefficient is nonzero, and introduces a bias to the signal correlation vector. Note, however that the spectrum of the signals at the point of combining, $Y_i(k)$, do not contain empty bands as in the case of full spectrum combining. Demodulating the subcarrier collapses all the data sidebands to baseband, allowing a much narrower combining bandwidth. Since the shared information rate for CSC is equal to the symbol rate, there is *no excess bandwidth that can be used to measure the correlation of the noise alone.* This problem may be solved by adding an extra matched filter for each receiver to capture noise only. Before investigating this possibility, however, we calculate the expectation of the noise product, $E[\tilde{N}_i(k)\tilde{N}_j^*(k)]$.

Consider the block diagram of Figure 5-1, which shows the processing for complex symbol combining up to the matched filter outputs. The signal $s_i(t)$ is the subcarrier

reference from the i^{th} subcarrier loop, given by

$$s_i(t) = \text{sqr}(\omega_{sc}t + \theta_{sc} + \phi_{sci}) \tag{5.3}$$

where θ_{sc} is the instantaneous subcarrier phase, and ϕ_{sc_i} is the instantaneous phase error in the i^{th} loop, for $i = 1 \ldots L$. The limits of integration for the i^{th} matched filter are given by

$$t_{l_i} = kT_s + \tau_i \tag{5.4}$$

$$t_{u_i} = (k+1)T_s + \tau_i \tag{5.5}$$

where τ_i is the timing error in the i^{th} symbol loop. The matched filter noise samples are therefore given by

$$\tilde{N}_i(k) = \frac{1}{T_s}\int_{kT_s+\tau_i}^{(k+1)T_s+\tau_i} \tilde{n}_i(t)\ \text{sqr}(\omega_{sc}t + \theta_{sc} + \phi_{sci})\ dt \tag{5.6}$$

$$\tilde{N}_j(k) = \frac{1}{T_s}\int_{kT_s+\tau_j}^{(k+1)T_s+\tau_j} \tilde{n}_j(t)\ \text{sqr}(\omega_{sc}t + \theta_{sc} + \phi_{scj})\ dt \tag{5.7}$$

The conditional expectation of $\tilde{N}_i(k)\tilde{N}_j^*(k)$ given the subcarrier and symbol timing errors can then be calculated by combining the above expressions with the cross-correlation function for the complex baseband noises, i.e.,

$$R_{\tilde{n}_i,\tilde{n}_j}(u,v) = E[\tilde{n}_i(u)\tilde{n}_j^*(v)] = \alpha_{ij}\, e^{j\phi_{ij}^n}\, \delta(u-v) \tag{5.8}$$

A delta function is used to express the cross-correlation for mathematical convenience. In reality, the cross correlation function takes the form $G(\tau)$, where $G(\tau)$ is determined by the shape of the front-end receiving filters (See Chapter 3). However, this approximation is justified, since the cross spectrum is essentially white over the bandwidth of interest (i.e., the data rate bandwidth $1/T_s$).

Using (5.6) - (5.8) yields

$$\begin{aligned} E[\tilde{N}_i(k)\tilde{N}_j^*(k)] &= \frac{1}{T_s^2} E\left[\int_{kT_s+\tau_i}^{(k+1)T_s+\tau_i} \int_{kT_s+\tau_j}^{(k+1)T_s+\tau_j} \tilde{n}_i(u)s_i(u)\ \tilde{n}_j^*(v)s_j(v)\ du\ dv\right] \\ &= \frac{\alpha_{ij}e^{j\phi_{ij}^n}}{T_s^2} \int_{kT_s+\tau_i}^{(k+1)T_s+\tau_i} \int_{kT_s+\tau_j}^{(k+1)T_s+\tau_j} \delta(u-v)\ s_i(u)s_j(v)\ du\ dv \\ &= \frac{\alpha_{ij}e^{j\phi_{ij}^n}}{T_s^2} \int_{t_{min}}^{t_{max}} s_i(v)s_j(v)\, dv \end{aligned} \tag{5.9}$$

where the limits of integration of v are given by

$$t_{min} = \max(kT_s + \tau_i,\ kT_s + \tau_j) \tag{5.10}$$

$$t_{max} = \min\left((k+1)T_s + \tau_i,\ (k+1)T_s + \tau_j\right) \tag{5.11}$$

Finally, integrating with respect to v yields

$$E[\tilde{N}_i(k)\tilde{N}_j^*(k)] = \frac{\alpha_{ij}e^{j\phi_{ij}^n}}{T_s^2}\left(1 - \frac{2}{\pi}|\phi_{sc_i} - \phi_{sc_j}|\right)\left(T_s - |\tau_i - \tau_j|\right) \tag{5.12}$$

$$= \frac{\alpha_{ij}e^{j\phi_{ij}^n}}{T_s}\left(1 - \frac{2}{\pi}|\phi_{sc_i} - \phi_{sc_j}|\right)\left(1 - \frac{1}{2\pi}|\phi_{sy_i} - \phi_{sy_j}|\right) \tag{5.13}$$

$$= \alpha_{ij}e^{j\phi_{ij}^n} R_{sym}\, C_{sc_{ij}}\, C_{sy_{ij}} \tag{5.14}$$

Note that in the absence of phase errors in any of the loops, (5.14) reduces to $\alpha_{ij}e^{j\phi_{ij}^n}R_{sym}$, which is simply the cross power spectral density of the noises $\tilde{n}_i(t)$ and $\tilde{n}_j(t)$ times the effective bandwidth of the matched filter. Thus, phase errors in the subcarrier and symbol loops actually reduce the observed noise correlation at the point of combining. This is in contrast to the case of full spectrum combining; since the signals are combined at the front end, the noise correlation is proportional to only the cross power spectral density level and the front-end bandwidth.

Calculating the unconditional covariance of the matched filter noises requires taking the expectation of (5.14) with respect to the phase errors $\phi_{sc_i}, \phi_{sc_j}, \phi_{sy_i}$, and ϕ_{sy_j}. Two approximations are made to perform this computation. First, the densities of the phase errors are assumed to be Gaussian. This condition is nearly satisfied for loop SNRs above 10 dB, and is consistent with the approximation made in [1]. Second,

the phase errors of all loops are assumed to be mutually independent. This statement is not strictly justifiable, since the subcarrier and symbol loops from a single receiver are affected by the same noise, and furthermore because the noises viewed by separate receivers are correlated. Nevertheless, it is invoked for the purpose of making a first-order approximation to evaluating the unconditional covariance. The quantities $\phi_{sc_i} - \phi_{sc_j}$ and $\phi_{sy_i} - \phi_{sy_j}$ are then Gaussian-distributed with known mean and variance, and the unconditional expectation $E[\tilde{N}_i(k)\tilde{N}_j^*(k)]$ becomes

$$\begin{aligned} E[\tilde{N}_i(k)\tilde{N}_j^*(k)] &= \alpha_{ij} e^{j\phi_{ij}^n} R_{sym}\, \overline{C_{sc_{ij}}}\, \overline{C_{sy_{ij}}} \\ &= \rho_{ij}\sqrt{N_{o_i}N_{o_j}}e^{j\phi_{ij}^n} R_{sym} \left(1 - \frac{2}{\pi}\sqrt{\frac{2}{\pi}}(\sigma^2_{\phi_{sc_i}} + \sigma^2_{\phi_{sc_j}})^{1/2}\right) \\ &\times \left(1 - \frac{1}{2\pi}\sqrt{\frac{2}{\pi}}(\sigma^2_{\phi_{sy_i}} + \sigma^2_{\phi_{sy_j}})^{1/2}\right) \end{aligned} \tag{5.15}$$

Equations (5.15) and (5.2) can be combined to calculate the ratio of the signal to noise correlation magnitude, analogous to that computed in (4.15):

$$\begin{aligned} \frac{|\vec{S}|}{|\vec{N}|} &= \frac{\sqrt{P_{D_1}P_{D_i}}\overline{C_{sc_1}}\,\overline{C_{sy_1}}\,\overline{C_{sc_i}}\,\overline{C_{sy_i}}}{\rho_{ij}\sqrt{N_{o_1}N_{o_i}}R_{sym}\overline{C_{sc_{ij}}}\,\overline{C_{sy_{ij}}}} \\ &\approx \frac{1}{\rho_{ij}}\left(\frac{E_{s_1}}{N_{o_1}}\frac{E_{s_i}}{N_{o_i}}\right)^{1/2} \end{aligned} \tag{5.16}$$

where $E_s/N_o = P_D T_s/N_o$ is the bit SNR. In making the approximation of (5.16), the effects of synchronization have been ignored for simplicity. This result provides a useful "rule of thumb" for determining if the noise correlation is a significant bias in estimating the relative signal phase. If $|\vec{S}|/|\vec{N}|$ is much less than one, then an extra correlation is needed to compensate for the noise vector, as mentioned earlier. On the other hand, if this quantity is much greater than one, then it is unnecessary to add the extra matched filter channel to perform the noise-only correlation. Estimating the degree of correlation ρ that will be observed for a particular antenna pair and applying the rule described above will indicate whether or not the noise contribution to the total correlation is substantial, and must be compensated for by performing

an additional correlation.

Here we briefly describe how the extra matched filter outputs can be used to measure the noise correlation: The complex baseband signal from each antenna can be shifted in frequency so that an empty portion of the spectrum is located at baseband. This may be accomplished by shifting by an even multiple of the subcarrier frequency, i.e.,

$$\begin{aligned}\tilde{y}_i'(t) &= \left(\sqrt{P_{C_i}}e^{j(\omega_b t+\theta_i)} + j\sqrt{P_{D_i}}d(t)\ \mathrm{sqr}(\omega_{sc}t+\theta_{sc})e^{j(\omega_b t+\theta_i)} + \tilde{n}_i(t)\right)e^{jN\omega_{sc}t} \\ &= \tilde{s}_i'(t) + \tilde{n}_i'(t) \end{aligned} \tag{5.17}$$

where N is an even integer. The shifted signal can then be multiplied by the subcarrier reference from the i^{th} antenna, and passed through a matched filter using timing from the i^{th} symbol loop, as shown in Figure 5-1. Thus,

$$\tilde{N}_i'(t) = \frac{1}{T_s}\int_{kT_s+\tau_i}^{(k+1)T_s+\tau_i} \tilde{n}_i'(t)\ \ \mathrm{sqr}(\omega_{sc}t+\theta_{sc}+\phi_{sc_i})\,dt \tag{5.18}$$

From the above analysis, it is clear that $E[\tilde{N}_i'(k)\tilde{N}_j'(k)]$ will be given by (5.15). Correlating the two noise-only matched filter outputs then yields a quantity that can be subtracted from the total correlation, Z, to compensate for the noise bias. The density function for the phase estimate computed using this technique is similar to the FSC case, and is analyzed in Appendix B. Note, however, that performing this compensation requires increasing the combining bandwidth beyond what is required for CSC in the uncorrelated noise case, as well as additional hardware to process the extra channel containing noise only. A tradeoff in performance versus complexity must therefore be made to determine if complex symbol combining is an attractive option when correlated noise is present.

5.2 Arrayed Symbol SNR and Symbol SNR Degradation

An expression for the conditional arrayed symbol SNR can be obtained in a similar manner as the full spectrum combining case. The combined signal for complex symbol combining is given by

$$\begin{aligned} \tilde{Y}_{comb}(k) &= \tilde{S}_{comb}(k) + \tilde{N}_{comb}(k) \\ &= \sum_{i=1}^{L} \beta_i e^{j\hat{\phi}_{1i}} \left(\sqrt{P_{D_i}} C_{sc_i} C_{sy_i}\, d(k)\, e^{(j\omega_b T_s k + \theta_i)} + \tilde{N}_i(k) \right) \end{aligned} \tag{5.19}$$

The conditional signal power, defined as $E[\tilde{S}_{comb}(k)]E[\tilde{S}^*_{comb}(k)]$, is given by

$$P'_D = P_{D_1}(\sum_{i=1}^{L} \gamma_i^2 C_{sc_i}^2 C_{sy_i}^2 + \sum_{i=1}^{L} \sum_{\substack{j=1 \\ i \neq j}}^{L} \gamma_i \gamma_j C_{sc_i} C_{sc_j} C_{sy_i} C_{sy_j}\, e^{j\psi_{ij}}\, e^{j(\Delta\phi_{1i} - \Delta\phi_{1i})}) \tag{5.20}$$

where, as before, $\Delta\phi_{1i}$ is defined as the error in estimating the phase difference between the 1^{st} and i^{th} signal, $\hat{\phi}_{1i} - \phi_{1i}$. The one-sided power spectral density of the real and imaginary parts of $\tilde{N}_{comb}(k)$ is given by

$$\begin{aligned} N'_o &= T_s\, Var\left(\tilde{N}_{comb}(k)\right) \\ &= T_s\, E\left[(\sum_{i=1}^{L} \beta_i e^{j\hat{\phi}_{1i}} \tilde{N}_i(k)) \times (\sum_{j=1}^{L} \beta_j e^{-j\hat{\phi}_{1j}} \tilde{N}^*_j(k)) \right] \end{aligned} \tag{5.21}$$

Using the relations

$$E[\tilde{N}_i(k)\tilde{N}^*_i(k)] = \frac{N_{o_i}}{T_s} \tag{5.22}$$

$$E[\tilde{N}_i(k)\tilde{N}^*_j(k)] = \frac{\rho_{ij}\sqrt{N_{o_i} N_{o_j}}\, e^{\phi^n_{ij}}}{T_s}\, C_{sc_{ij}}\, C_{sy_{ij}} \tag{5.23}$$

Equation (5.21) can be shown to be equal to

$$N'_o = N_{o_1}(\sum_{i=1}^{L} \gamma_i + \sum_{i=1}^{L} \sum_{\substack{j=1 \\ i \neq j}}^{L} \sqrt{\gamma_i \gamma_j}\, \rho_{ij} C_{sc_{ij}} C_{sy_{ij}}\, e^{j\psi_{ij}} e^{j(\Delta\phi_{1i} - \Delta\phi_{1j})} \tag{5.24}$$

Taking the ratio of (5.20) to (5.24) then yields the combined P_D/N_o for CSC. The combined signal is finally processed by a baseband Costas loop, and the conditional SNR adding in carrier losses is given by

$$SNR' = \frac{2P_{D_1}}{N_{o_1}R_{sym}} \frac{\sum_{i=1}^{L}\gamma_i^2 C_{sc_i}^2 C_{sy_i}^2 + \sum_{i=1}^{L}\sum_{\substack{j=1\\i\neq j}}^{L}\gamma_i\gamma_j C_{sc_i}C_{sc_j}C_{sy_i}C_{sy_j}e^{j(\Delta\phi_{1i}-\Delta\phi_{1j})}}{\sum_{i=1}^{L}\gamma_i + \sum_{i=1}^{L}\sum_{\substack{j=1\\i\neq j}}^{L}\sqrt{\gamma_i\gamma_j}\rho_{ij}C_{sc_{ij}}C_{sy_{ij}}e^{j\psi_{ij}}e^{j(\Delta\phi_{1i}-\Delta\phi_{1j})}} C_c^2 \tag{5.25}$$

Computing the unconditional symbol SNR requires taking the expectation of the above quantity with respect to the phase errors ϕ_{sc_i} and ϕ_{sy_i} for $i = 1 \ldots L$, the phase estimates $\hat{\phi}_{1i}$ for $i = 2 \ldots L$, and the carrier phase error ϕ_c. Once again, we assume all loop phase errors and phase-aligning errors are mutually independent. Thus, integration over the carrier phase error ϕ_c is accomplished easily by considering the carrier reduction function C_c^2 separately. However, unlike the case of full spectrum combining, the subcarrier and symbol phase errors appear in both the numerator *and* the denominator. The expectation with respect to the subcarrier and symbol phase errors therefore cannot be given in closed form. Calculating the unconditional symbol SNR for even a simple two-element array would thus require a 5^{th} order numerical integration. Rather than resort to such brute-force tactics, we make further simplifying assumptions to allow evaluation of some of the integrals in closed form.

In taking expectation with respect to the ϕ_{sc_i} and ϕ_{sy_i} terms, we apply the approximation

$$E[\frac{x}{y}] \approx \frac{E[x]}{E[y]} \tag{5.26}$$

to the ratio of (5.25), yielding

$$SNR = \frac{2P_{D_1}}{N_{o1}R_{sym}} E_{\hat{\Phi}}\left[\frac{E_{\Phi_{sc},\Phi_{sy}|\hat{\Phi}}[\sum_{i=1}^{L}\gamma_i^2 C_{sc_i}^2 C_{sy_i}^2 + \sum_{i=1}^{L}\sum_{\substack{j=1\\i\neq j}}^{L}\gamma_i\gamma_j C_{sc_i}C_{sc_j}C_{sy_i}C_{sy_j}e^{j(\Delta\phi_{1i}-\Delta\phi_{1j})}]}{E_{\Phi_{sc},\Phi_{sy}|\hat{\Phi}}[\sum_{i=1}^{L}\gamma_i + \sum_{i=1}^{L}\sum_{\substack{j=1\\i\neq j}}^{L}\sqrt{\gamma_i\gamma_j}\rho_{ij}C_{sc_{ij}}C_{sy_{ij}}e^{j\psi_{ij}}e^{j(\Delta\phi_{1i}-\Delta\phi_{1j})}]}\right]\overline{C_c^2} \tag{5.27}$$

where Φ_{sc} is the set of subcarrier phase errors ϕ_{sc_i} for $i = 1 \ldots L$, Φ_{sy} is the set of

symbol phase errors ϕ_{sy_i} for $i = 1 \ldots L$, and $\hat{\Phi}$ is the set of phase estimates $\hat{\phi}_{1i}$ for $i = 2 \ldots L$. The approximation of (5.26) is reasonable if the mean of y squared is much greater than the variance of y (i.e., if y is nearly a constant). This condition is met for the case under consideration, since it is implicitly assumed that the loop SNRs of the subcarrier and symbol loops are high enough to maintain lock, with 13 dB being a typical threshold. Thus, the variances of the reduction functions $C_{sc_{ij}}$ and $C_{sy_{ij}}$, which contain the loop phase errors, will be small compared to the mean of the entire denominator term.

By the above argument, the unconditional SNR can be evaluated as

$$SNR = \frac{2P_{D_1}}{N_{o_1} R_{sym}} \overline{C_c^2} \int_{-\pi}^{\pi} \cdots \int_{-\pi}^{\pi} \left[\frac{\sum_{i=1}^{L} \gamma_i^2 \overline{C_{sc_i}^2}\ \overline{C_{sy_i}^2} + \sum_{i=1}^{L} \sum_{\substack{j=1 \\ i \neq j}}^{L} \gamma_i \gamma_j \overline{C_{sc_i}}\ \overline{C_{sc_j}}\ \overline{C_{sy_i}}\ \overline{C_{sy_j}} e^{j(\Delta\phi_{1i} - \Delta\phi_{1j})}}{\sum_{i=1}^{L} \gamma_i + \sum_{i=1}^{L} \sum_{\substack{j=1 \\ i \neq j}}^{L} \sqrt{\gamma_i \gamma_j} \rho_{ij} \overline{C_{sc_{ij}}}\ \overline{C_{sy_{ij}}} e^{j\psi_{ij}} e^{j(\Delta\phi_{1i} - \Delta\phi_{1j})}} \right.$$
$$\left. p(\Delta\phi_{12}) \cdots p(\Delta\phi_{1L}) \right] d\Delta\phi_{12} \cdots d\Delta\phi_{1L} \tag{5.28}$$

The ideal symbol SNR for complex symbol combining is identical to that for full spectrum combining; since SNR_{ideal} is defined as the SNR that would be obtained in the absence of synchronization errors, its value is independent of what order combining and demodulation occur in. Thus, the degradation for complex symbol combining is found by combining the results of (5.28) with (4.11), yielding

$$D_{csc} = \overline{C_c^2} \int_{-\pi}^{\pi} \cdots \int_{-\pi}^{\pi} \left[\frac{\sum_{i=1}^{L} \gamma_i^2 \overline{C_{sc_i}^2}\ \overline{C_{sy_i}^2} + \sum_{i=1}^{L} \sum_{\substack{j=1 \\ i \neq j}}^{L} \gamma_i \gamma_j \overline{C_{sc_i}}\ \overline{C_{sc_j}}\ \overline{C_{sy_i}}\ \overline{C_{sy_j}} e^{j(\Delta\phi_{i1} - \Delta\phi_{j1})}}{\sum_{i=1}^{L} \gamma_i + \sum_{i=1}^{L} \sum_{\substack{j=1 \\ i \neq j}}^{L} \sqrt{\gamma_i \gamma_j} \rho_{ij} \overline{C_{sc_{ij}}}\ \overline{C_{sy_{ij}}} e^{j\psi_{ij}} e^{j(\Delta\phi_{i1}^n - \Delta\phi_{j1}^n)}} \right.$$
$$\left. p(\Delta\phi_{12}) \cdots p(\Delta\phi_{1L}) \right] d\Delta\phi_{12} \cdots d\Delta\phi_{1L}\, G_A^{-1} \tag{5.29}$$

5.3 Simulation Results

Simulations of a two-antenna complex symbol combining system were performed. The signal parameters used were the same as those used for the full spectrum combining

simulations: $P_{T_1}/N_{o_1} = P_{T_2}/N_{o_2} = 25$ dB-Hz, $R_{sym} = 200$ sps, and $\Delta = 90°$. The loop bandwidths were also set as before; the carrier, subcarrier, and symbol loop bandwidths were 3.5 Hz, 0.75 Hz, and 0.15 Hz, respectively, with a symbol window of 1/2. Both the compensating and non-compensating methods of estimating the signal phase difference were implemented. In Figures 5-2 and 5-3, simulated and analytical degradation values are shown for various values of ρ and ψ.

For the uncompensated case, the degradation curve drops down sharply for $\psi = 90°$ and $\psi = 180°$. One cause for this is the bias in the complex correlation used to estimate the relative signal phase. For the parameters being used, $|\vec{S}|/|\vec{N}|$, given by (5.16), is equal to 3.15 for $\rho = 0.5$. Thus, the noise vector is of comparable but lesser magnitude to that of the signal in estimating the phase. Note that for $\psi = 0°$, the noise correlation phase is equal to the relative signal phase ($\phi = \phi^n$), and the vectors $\vec{S}$ and $\vec{N}$ are colinear (see Figure 4-3). The noise vector therefore does not bias the measurement away from the desired quantity, and the downward trend is not present.

For the compensated case, less overall degradation is observed. However, the $\psi = 180°$ curve still drops down with increasing ρ. Recall from Sec. 5.1 that imperfect subcarrier and symbol tracking tend to decrease the power levels of the individual signals at the matched filter output *and* decrease the correlation of the matched filter noises. When $\psi = 0°$, this has a beneficial effect on the arrayed SNR, since it reduces the coherent addition of the noise. By contrast, when $\psi = 180°$, a high degree of correlation between the noises is desirable, so that the noise cancels maximally. Thus, decreasing this correlation lessens the arrayed SNR, and causes more degradation. This explains the fact that the $\psi = 0°$ curve tends upwards with increasing ρ, while the $\psi = 180°$ tends downward. Note, however, that the reverse trend is true of the ideal arraying gain, G_A. For example, for $\rho = 0.8$, $G_A = 10$ dB for $\psi = 180°$, but only 0.46 dB for $\psi = 0°$.

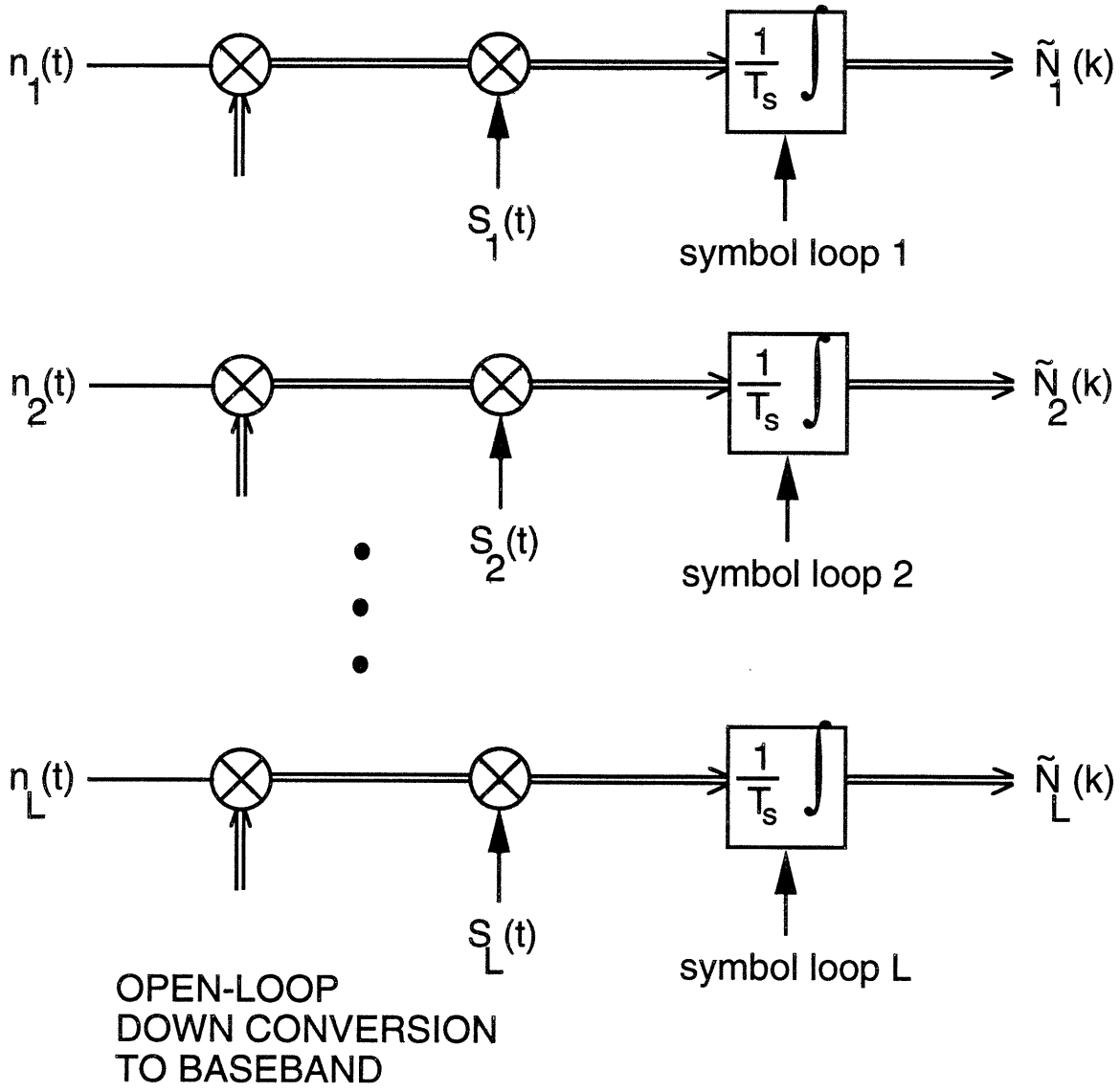

Figure 5-1: Matched filter noise outputs for CSC

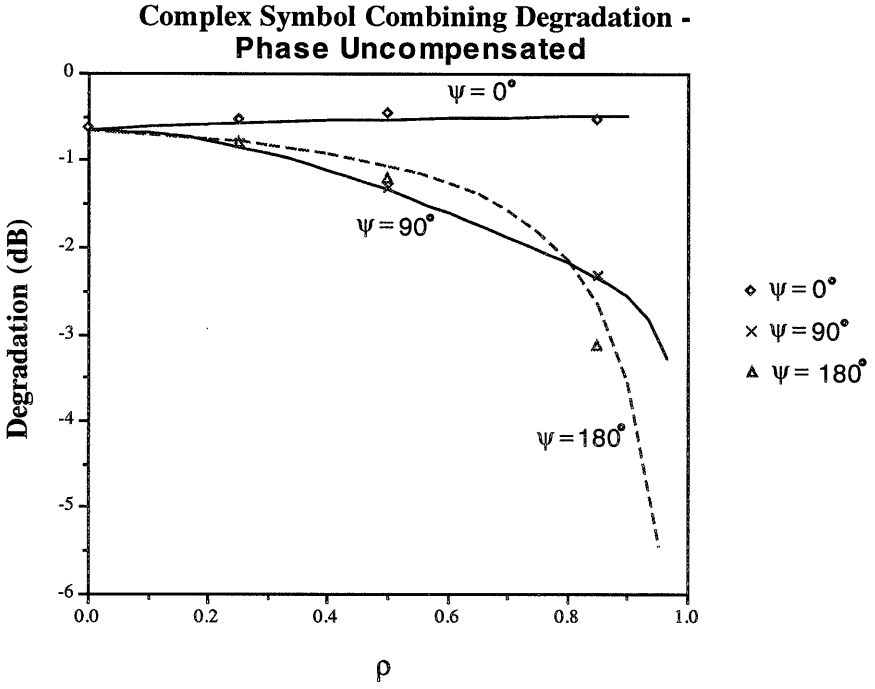

Figure 5-2: CSC degradation - theory and simulation

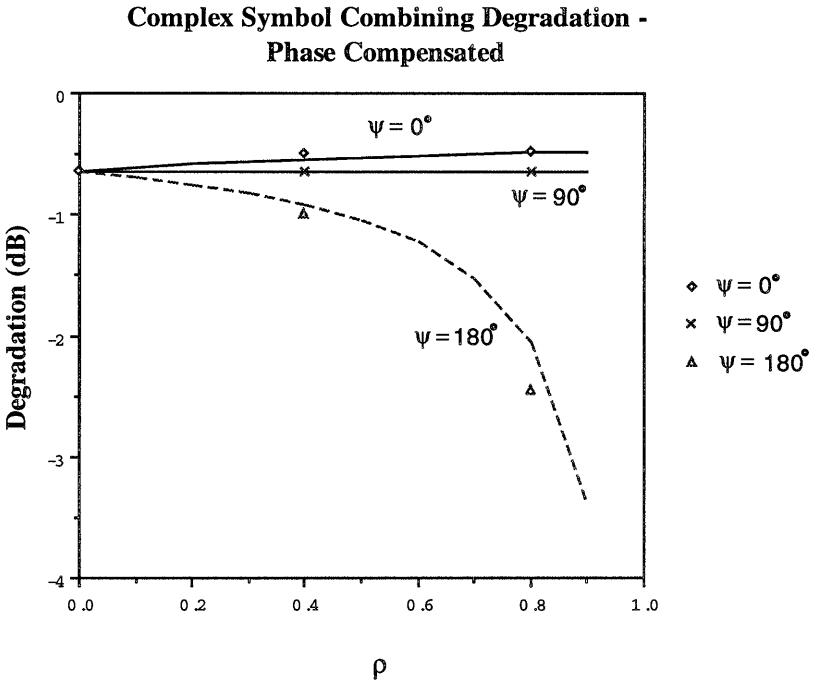

Figure 5-3: CSC degradation - theory and simulation

Chapter 6

Analysis of Full-Spectrum and Complex-Symbol Combining for Galileo Mission and Conclusion

In order to illustrate the major concepts presented in this thesis, the performance of full spectrum combining and complex symbol combining is analyzed for the Galileo signal. An array of DSS-14, which is a 70 m antenna, and DSS-15, a 34 m high-efficiency (HEF) antenna, is chosen for this example. First, predictions for physical parameters describing the signal strength and degree of noise correlation are developed. These quantities are then used to calculate the arraying gain and degradation for each of the two schemes. Finally, the conclusion summarizes the major issues related to telemetry arraying in the presence of correlated noise.

6.1 Galileo Signal Parameters

In the case of the Galileo spacecraft, correlated noise will be contributed by Jupiter being in the beam of both antennas. As discussed in Section 2, the contribution of a background body to total system noise depends on its angular separation from the spacecraft and on its total flux, which varies with its distance from Earth. Values for the Jupiter-Earth-probe (JEP) angle and Jupiter-Earth distance can be found

from ephemeris information for the Galileo tour. For the purpose of this example, we select values which maximize the noise contribution of the planet to estimate the impact of correlated noise in a worst-case scenario. Thus, we assume the JEP angle is zero and that the Jupiter-Earth range is at its minimum value during the tour, which is $R_j = 4.0$ au [1]. Using these values, the temperature contribution of Jupiter for DSS-14 and DSS-15 are $T_{s_1} = 6.6K$ and $T_{s_2} = 1.4K$, respectively. Note that the temperature contribution is higher for DSS-14 due to the greater aperture size and antenna efficiency.

The predicted signal parameters are as follows: $(\frac{P_T}{N_o})_1 = 22.0$ dB Hz and $(\frac{P_T}{N_o})_2 = 11.6$ dB Hz for the 70- and 34-m antennas, respectively; $\Delta = 90°$; and $R_{sym} = 200$ sps. Note that since we are assuming that the planet and spacecraft are at their closest range, the spacecraft signal is *also* at its peak strength, in addition to the noise contribution of Jupiter. The total system temperatures predicted for DSS-14 and DSS-15 are 22.6 K and 42.2 K, respectively.[2]

To determine the degree to which the source is resolved on this array baseline, we must compare the fringe spacing to the angular size of the source. In our example, the observing frequency f_o is $2.3 \times 10^9 Hz$, and the maximum possible projected baseline is the physical separation between the two antennas, which is approximately 500 m. Thus, the smallest possible fringe spacing is 2.5×10^{-4} rad. At a range of 4.0 au, Jupiter has an angular size on the order of 1×10^{-3} rad. Since these values are comparable, we cannot use either the long baseline limit or the short baseline limit in evaluating ρ (see Section 1). However, for the purpose of determining the impact of the correlated noise in the most extreme case, we over-estimate the degree of noise correlation using the upper bound on ρ, given by

$$\rho = \sqrt{\frac{T_{s_1} T_{s_2}}{T_1 T_2}} \approx 0.1 \tag{6.1}$$

[1]The unit 'au' stands for astronomical units, which is a measure of distance frequently used for interplanetary navigation purposes.

[2]Predictions for noise and signal parameters were obtained from the Galileo S-Band Analysis Program, courtesy of David Bell.

6.2 Arraying Performance

Using the two P_T/N_o levels and correlation coefficient ρ found above, the ideal arraying gain G_A can be computed as a function of ψ using (4.11). A graph showing this relationship is shown in Figure 6.2. Note that the arraying gain in this example is

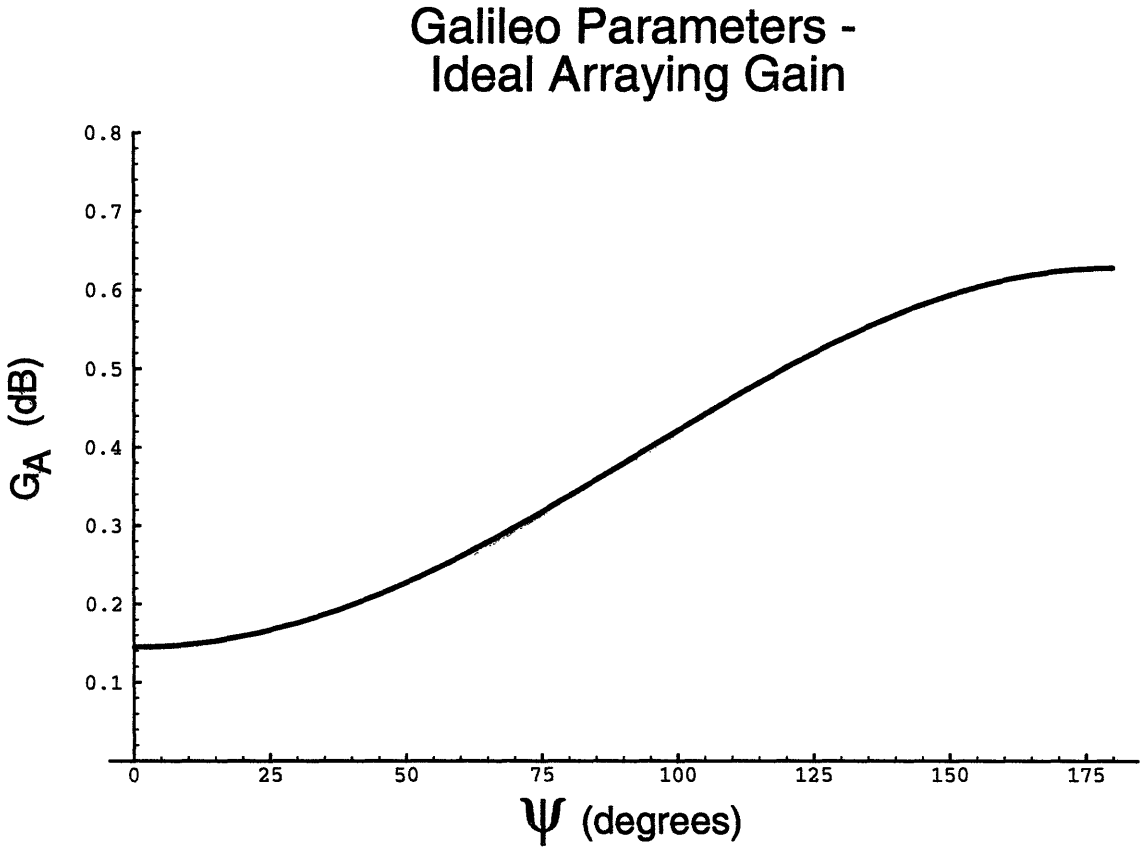

Figure 6-1: Ideal arraying gain for Galileo signal, array of DSS-14 and DSS-15

much smaller compared to our previous examples of two equal antennas, since the signal level of one antenna is approximately 10 dB lower than the other. For $\psi = 0°$, the correlated component of the noise adds maximally in phase, thus decreasing the arraying gain. By contrast, the background noise interferes destructively for $\psi = 180°$, resulting in greater arraying gain. Since the correlation coefficient is relatively low in this example, the difference between the best-case and worst-case scenario is only about 0.45 dB.

Representative values for the carrier, subcarrier, and symbol loop bandwidths were

chosen as 1.5 Hz, 0.4 Hz, and 0.07 Hz, respectively. For full-spectrum combining, a correlation bandwidth of $B_{corr} = 2$ kHz was used, with a correlation time of 15 seconds. The total degradation for FSC as a function of ψ is shown in Figure 6.2, along with simulation points. Because the correlation coefficient ρ is relatively low in this example, the degradation is almost constant with respect to the phase parameter ψ. The combined P_T/N_o only varies by roughly 0.4 dB as ψ ranges from 0° to 180°; thus, the loop SNRs of the three loops also do not change much, and synchronization losses remain essentially constant.

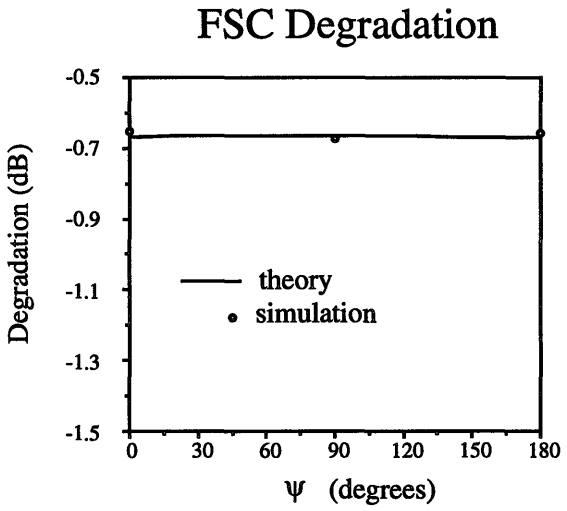

Figure 6-2: FSC performance for Galileo signal

The same signal parameters and loop bandwidths were used to simulate the complex symbol combining case. A slight variation of the basic scheme, known as complex symbol combining with aiding (CSCA), was implemented. This scheme is discussed in [2] as an option for arraying the Galileo signal. In CSCA, the subcarrier and symbol references from the receiver tracking the stronger signal are used to track the signal from the 34 m antenna as well. This technique can be used to perform complex symbol combining even if the 34 m antenna signal is too weak to achieve subcarrier and symbol lock on its own. Thus, the loop SNRs for the 34 m antenna subcarrier and symbol loops are equal to the corresponding 70 m antenna loop SNRs.

Equation (5.16) can be applied to determine whether or not the "noise-only"

channel is needed to phase the array. Substituting in values from above, we find

$$\frac{1}{\rho}\left(\frac{E_{s_1}}{N_{o_1}}\frac{E_{s_2}}{N_{o_2}}\right)^{1/2} = \frac{1}{\rho}\frac{1}{R_{sym}}\left(\frac{P_{T_1}}{N_{o_1}}\frac{P_{T_2}}{N_{o_2}}\right)^{1/2} \quad (6.2)$$

$$= 2.39 \quad (6.3)$$

Thus, the magnitude of the noise correlation vector is less than but comparable to that of the signal correlation vector. To illustrate the impact of the phase bias in aligning the signals, CSCA was simulated with both the compensating and uncompensating method for estimating the relative signal phase. In Figure 6.2, we show the degradation for CSCA for these two cases. The correlation time used to estimate the relative signal phase was 2 seconds. Note that a shorter estimation interval than the full spectrum combining case can be used here, since the effective correlation bandwidth is equal to the data bandwidth of 200 Hz as opposed to 2 kHz for FSC. For the compensated case, the degradation is essentially constant, since, once again, the noise correlation does not affect synchronization losses much. For the uncompensated case, the degradation becomes greater as the difference between the noise and signal phase ψ grows larger, since the noise correlation begins to bias the phase estimate further away from the relative signal phase. This effect can be seen graphically by referring once again to Figure 4-3, where the complex signal and noise correlations are represented as vectors.

6.3 Conclusion

The effects of correlated noise on the full spectrum combining and complex symbol combining arraying schemes have been analyzed. For both schemes, there are substantial differences from the case of arraying signals with uncorrelated noise. The importance of these factors depends on the degree of noise correlation, quantified by the correlation coefficients ρ_{ij} for the various antenna pairs in the array. As seen in Chapter 3, accurate modeling of the noise correlation properties for a given antenna pair requires detailed analysis of factors such as the source structure and position,

the antenna gain patterns, and the geometry of the array. However, the correlation coefficient can be determined easily in cases where the baseline is either very short or very long. These two extreme cases can be used to obtain a rough idea of what degree of noise correlation can be expected for a given scenario.

The ideal arraying gain for a set of signals, G_A, is maximum SNR improvement over the strongest signal in the array that can be achieved through combining. Since G_A does not account for losses due to imperfect synchronization, it is useful for describing the performance of arraying in general, but not for comparing specific algorithms for arraying. For a given set of correlation coefficients ρ_{ij}, the ideal arraying gain may be lower *or* higher than the case of uncorrelated noise waveforms. This reflects the fact that the noise may add constructively or destructively, depending on the relative signal and noise phases (i.e., the ψ_{ij} parameters).

Correlated noise also has an impact on the symbol SNR degradation for individual arraying schemes, which quantify the amount of synchronization loss incurred based on specific processing used. One major difference from the uncorrelated noise case is in the phase alignment process. Both full spectrum combining and complex symbol combining use correlations between the various signal pairs to estimate the difference in carrier phases. When the noise waveforms are non-independent, the noise products contribute to the total measured correlation, producing a bias in the estimated phase. The magnitude of the noise correlation relative to the signal correlation can be computed from the signal levels (i.e., the $P_T/N_o's$), the degree of noise correlation, and the correlation bandwidths used. Since the contribution of the noise bias is proportional to the correlation bandwidth used, full spectrum combining is more severely affected by this problem than complex symbol combining. A modified method of phase estimation, where the correlation due to the noise alone is measured and compensated for, can optionally be employed for both FSC and CSC, as necessary.

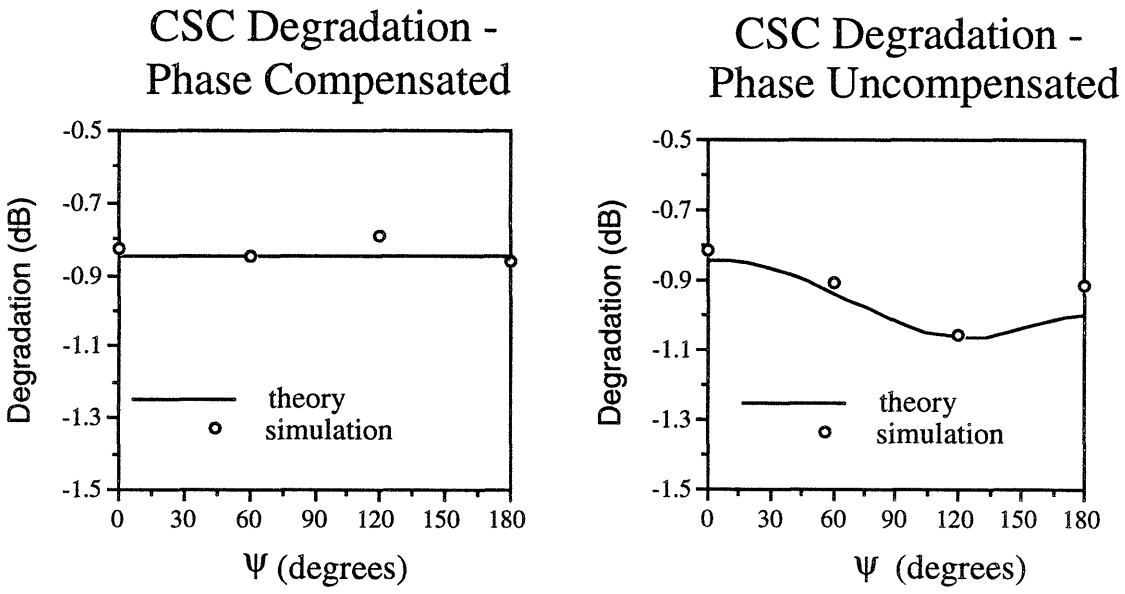

Figure 6-3: CSC performance for Galileo signal

Appendix A

Performance of the FSC Correlator

For full spectrum combining, the phase difference between two signals is estimated by performing one lowpass and one bandpass correlation, as described in Section 3.2. After being filtered to some lowpass bandwidth B_{lp} Hz, the signals from antenna 1 and antenna i are given by

$$\tilde{y}_{lp_1}(t) = \left[\sqrt{P_{C_1}} + j\sqrt{P_{D_1}}d(t)\left(\frac{4}{\pi}\right)\sum_{\substack{k=1\\ k\ odd}}^{M}\frac{\sin k\omega_{sc}t}{k}\right]e^{(j\omega t+\theta_1)} + \tilde{n}_{lp_1}(t) \quad \text{(A.1)}$$

$$\tilde{y}_{lp_i}(t) = \left[\sqrt{P_{C_i}} + j\sqrt{P_{D_i}}d(t)\left(\frac{4}{\pi}\right)\sum_{\substack{k=1\\ k\ odd}}^{M}\frac{\sin k\omega_{sc}t}{k}\right]e^{(j\omega t+\theta_i)} + \tilde{n}_{lp_i}(t) \quad \text{(A.2)}$$

where the subcarrier is expressed in terms of its sinusoidal components that are passed by the lowpass filter. The two signals passed through the bandpass filter of bandpass B_{bp} Hz contain only noise, and are given by

$$\tilde{y}_{bp_1}(t) = \tilde{n}_{bp_1}(t) \quad \text{(A.3)}$$

$$\tilde{y}_{bp_i}(t) = \tilde{n}_{bp_i}(t) \quad \text{(A.4)}$$

The complex quantity used to estimate the relative signal phase $\phi_{1i} = \theta_1 - \theta_i$ is

given by

$$\begin{aligned} Z &= I + jQ \\ &= \frac{1}{T_{corr}} \int \tilde{y}_{lp_1} \tilde{y}^*_{lp_i}\, dt - \frac{B_{lp}}{B_{bp}} \frac{1}{T_{corr}} \int \tilde{y}_{bp_1} \tilde{y}^*_{bp_i}\, dt \\ &= (\sqrt{P_{C_1} P_{C_i}} + \sqrt{P_{D_1} P_{D_i}} H) e^{j\phi_{1i}} + \frac{1}{T_{corr}} \int (\tilde{n}_{s,n} + \tilde{n}_{lp_1} \tilde{n}^*_{lp_i})\, dt \\ &\quad - \frac{B_{lp}}{B_{bp}} \frac{1}{T_{corr}} \int \tilde{n}_{bp_1} \tilde{n}^*_{bp_i}\, dt \\ &= (\sqrt{P_{C_1} P_{C_i}} + \sqrt{P_{D_1} P_{D_i}} H) e^{j\phi_{1i}} + \tilde{N} \end{aligned} \tag{A.5}$$

In most cases, the contribution of the signal-noise term $\tilde{n}_{s,n}(t)$ to the total noise power is much smaller than that of the noise-noise terms, and can be ignored. This is especially true if the P_T/N_o levels of the two signals are very low, or if large correlation bandwidths are used. By the Central Limit Theorem, the complex noise $\tilde{N}$ can be approximated as Gaussian if the correlation extends over many independent samples (i.e., if T_{corr} is much greater than the inverse correlation bandwidths). After averaging, the variance of the real and imaginary parts of $\tilde{N}$ can be shown to be equal to

$$\lambda_I = Var(N_I) = \frac{1}{T_{corr}} \left(B_{lp} + \frac{B^2_{lp}}{B_{bp}} \right) (N_{o_1} N_{o_i} + \alpha^2_{1i} \cos 2\phi^n_{1i}) \tag{A.6}$$

$$\lambda_Q = Var(N_Q) = \frac{1}{T_{corr}} \left(B_{lp} + \frac{B^2_{lp}}{B_{bp}} \right) (N_{o_1} N_{o_i} - \alpha^2_{1i} \cos 2\phi^n_{1i}) \tag{A.7}$$

where N_I and N_Q are the real and imaginary parts of $\tilde{N}$, respectively. The covariance of N_I and N_Q can be shown to be equal to

$$\lambda_{IQ} = Cov(N_I,\, N_Q) = \frac{1}{T_{corr}} \left(B_{lp} + \frac{B^2_{lp}}{B_{bp}} \right) \alpha^2_{1i} \sin 2\phi^n_{1i} \tag{A.8}$$

Furthermore, it is clear from (A.5) that the means of the real and imaginary parts of Z are given by

$$m_I = (\sqrt{P_{C_1} P_{C_i}} + \sqrt{P_{D_1} P_{D_i}} H) \cos \phi_{1i} \tag{A.9}$$

$$m_Q = (\sqrt{P_{C_1}P_{C_i}} + \sqrt{P_{D_1}P_{D_i}}H)\sin\phi_{1i} \tag{A.10}$$

Equations (A.6), (A.7), (A.9), and (A.10) can be combined to compute the correlator SNR as defined in [1], i.e.,

$$\begin{aligned} SNR_{corr,fsc} &= \frac{E[Z]E^*[Z]}{E[ZZ^*] - E[Z]E^*[Z]} \\ &= \frac{m_I^2 + m_Q^2}{\lambda_I + \lambda_Q} \\ &= \frac{T_{corr}}{2(B_{lp} + \frac{B_{lp}^2}{B_{bp}})}\left(\sqrt{\frac{P_{C_1}}{N_{o_1}}\frac{P_{C_i}}{N_{o_i}}} + \sqrt{\frac{P_{D_1}}{N_{o_1}}\frac{P_{D_i}}{N_{o_i}}}H\right)^2 \end{aligned} \tag{A.11}$$

Equations (A.9), (A.10), and (A.6) - (A.8) can be used to determine the joint density function $p_{I,Q}(I,Q)$. Since the density of $\hat{\phi}_{1i} = \tan^{-1}\left(\frac{Q}{I}\right)$ is the desired quantity, we express the joint density function in terms of polar coordinates, using the variable definitions

$$r \triangleq \sqrt{I^2 + Q^2} \tag{A.12}$$

$$\phi \triangleq \tan^{-1}\left(\frac{Q}{I}\right) \tag{A.13}$$

The density function for jointly Gaussian random variables is given in polar form by

$$f_{r,\phi}(r,\phi) = \frac{r}{2\pi(\lambda_I\lambda_Q - \lambda_{IQ})} \times \exp\left(-\frac{\lambda_I(r\cos\phi - m_I)^2 - 2\lambda_{IQ}(r\cos\phi - m_I)(r\sin\phi - m_Q) + \lambda_Q(r\sin\phi - m_Q)^2}{2(\lambda_I\lambda_Q - \lambda_{IQ})}\right) \tag{A.14}$$

Integrating (A.14) with respect to r yields the marginal density of ϕ alone. Expressing

the phase estimate density in terms of the estimation error $\Delta\phi = \hat{\phi}_{1i} - \phi_{1i}$ yields

$$f_\phi(\Delta\phi) = G_1 \exp\left(-SNR_{corr,fsc}\frac{1-\rho^2\cos 2\psi}{1-\rho^4}\right)\left[1+\sqrt{\pi}\,G_2\,e^{G_2^2}\,(\mathrm{erf}\,G_2+1)\right] \quad \text{(A.15)}$$

where

$$G_1 = \frac{1-\rho^4}{2\pi\,(1-\rho^2\cos(2\psi-\Delta\phi))} \quad \text{(A.16)}$$

$$G_2 = \sqrt{SNR_{corr,fsc}}\frac{\cos\Delta\phi-\rho^2\cos(2\psi-\Delta\phi)}{(1-\rho^4)(1-\rho^2\cos(2\psi-\Delta\phi))} \quad \text{(A.17)}$$

Appendix B

Performance of the CSC Correlator

The method of estimating the relative signal phases for complex symbol combining is analogous to the full spectrum combining algorith; using the extra correlation to compensate for the noise bias, the complex correlation can be expressed as

$$\begin{aligned} Z &= \frac{1}{N}\sum_{k=1}^{N}\tilde{Y}_1(k)\tilde{Y}_i^*(k) - \frac{1}{N}\sum_{k=1}^{N}\tilde{N}_1(k)\tilde{N}_i^*(k) \\ &= \sqrt{P_{D_1}P_{D_i}\overline{C_{sc_1}}\,\overline{C_{sy_1}}\,\overline{C_{sc_i}}\,\overline{C_{sy_i}}}e^{j\phi_{1i}} + \frac{1}{N}\sum_{k=1}^{N}\sqrt{P_{D_1}}C_{sc_1}C_{sy_1}e^{j\theta_1}\tilde{N}_i^*(k) \\ &\quad + \frac{1}{N}\sum_{k=1}^{N}\sqrt{P_{D_i}}C_{sc_i}C_{sy_i}e^{-j\theta_i}\tilde{N}_1^*(k) + \frac{1}{N}\sum_{k=1}^{N}\tilde{N}_1(k)\tilde{N}_i^*(k) - \frac{1}{N}\sum_{k=1}^{N}\tilde{N}_1'(k)\tilde{N}_i'^*(k) \\ &= \sqrt{P_{D_1}P_{D_i}\overline{C_{sc_1}}\,\overline{C_{sy_1}}\,\overline{C_{sc_i}}\,\overline{C_{sy_i}}}e^{j\phi_{1i}} + \tilde{N} \end{aligned} \tag{B.1}$$

where N is the number of symbols averaged over, given by $N = T_{corr}/T_{sym}$, and the noise term $\tilde{N}$ has zero mean. The statistics of this noise can be analyzed in the same manner as before; here, the effective correlation bandwidth for both the lowpass and the bandpass correlation is $R_{sym}/2$. Using the definition given by (4.18), the correlator SNR can be shown to be equal to

$$SNR_{corr,csc} = \frac{P_{D_1}}{N_{o_1}}\frac{T_{corr}\overline{C_{sc_1}}^2\,\overline{C_{sy_1}}^2\,\overline{C_{sc_i}}^2\,\overline{C_{sy_i}}^2}{\overline{C_{sc_i}^2}\,\overline{C_{sy_i}^2} + \overline{C_{sc_1}^2}\,\overline{C_{sy_1}^2}\left(\frac{1}{\gamma_i}\right) + \frac{N_{o_i}}{P_{D_i}}2R_{sym}} \tag{B.2}$$

The density function for the phase estimation error can be found in an analogous manner as applied in Appendix A. The only difference is in the expression for the correlator SNR; otherwise, both problems are governed by the same mathematics. The density function for the phase estimation error $\Delta\phi_{1i}$ is thus given by (A.15), with $SNR_{corr,fsc}$ replaced by $SNR_{corr,csc}$.

Bibliography

[1] A. Mileant and S. Hinedi, "Overview of Arraying Techniques for Deep Space Communications," *IEEE Transactions on Communications*, Vol. 42, No. 2/3/4, pp. 1856 - 1865, February/March/April 1994.

[2] S. Million, B. Shah, and S. Hinedi, "A Comparison of Full-Spectrum and Complex-Symbol Combining Techniques for the Galileo S-Band Mission," *Telecommunication and Data Acquisition Progress Report 42-116* Jet Propulsion Laboratory, Pasadena, California, pp. 128-162, February 15, 1994.

[3] R. Dewey, "The Effects of Correlated Noise in Intra-Complex DSN Arrays for S-Band Galileo Telemetry Reception," *Telecommunication and Data Acquisition Progress Report 42-111*, Jet Propulsion Laboratory, Pasadena, California, p. 129 - 152, November 15 1992.

[4] R. Gagliardi, *Introduction to Communications Engineering*, John Wiley & Sons, New York, New York, 1988.

[5] G. Resch, "Jupiter's Contribution to the Total System Temperature at S-Band During the Galileo Mission," Interoffice Memorandum # 335.3-92.02, Jet Propulsion Laboratory, Pasadena, California, June 23, 1993.

[6] A. Thompson, J. Moran, and G. Swenson, *Interferometry and Synthesis in Radio Astronomy*, John Wiley & Sons, New York, 1986.

[7] H. Tan, "Optimum Weight Coefficients for Array Feed Combining of Broadband Signals in Correlated Noise," to appear in *Telecommunication and Data Acqui-*

sition Progress Report 42-121, Jet Propulsion Laboratory, Pasadena, California, May 15, 1995.